Mechanism of Inhibition of the Human Sirtuin Deacetylase SIRT3: Computational and Experimental Studies

Xiangying Guan[1], Eric Knoll[1], Ping Lin[1], and Raj Chakrabarti[1, 2*]

[1]Division of Fundamental Research, PMC Advanced Technology, LLC, NJ 08054, USA

[2] Department of Chemical Engineering and

Center for Advanced Process Decision-Making, College of Engineering,

Carnegie Mellon University, PA 15213, USA

* To whom correspondence should be addressed:

Raj Chakrabarti, Ph.D.

Associate Professor of Chemical Engineering

Department of Chemical Engineering

Center for Advanced Process Decision-Making

College of Engineering

Carnegie Mellon University

Doherty Hall 3122

5000 Forbes Avenue

Pittsburgh, PA 15213

Phone: (609) 216-4644

Email: rajc@andrew.cmu.edu

raj@pmc-group.com

Abstract

Sirtuins are key regulators of many cellular functions including cell growth, apoptosis, metabolism, and genetic control of age-related diseases. Sirtuins are themselves regulated by their cofactor nicotinamide adenine dinucleotide (NAD^+) as well as by their reaction product nicotinamide (NAM), the concentrations of which vary during the aging process. The mechanism of inhibition of human SIRT3, the major mitochondrial sirtuin, by nicotinamide and its analogues was investigated *in vitro* and *in silico* and compared to those of Sir2 and human SIRT1, using experimental kinetic analysis as well as Molecular Mechanics-Poisson Boltzmann/Generalized Born Surface Area (MM-PB(GB)SA) calculations with molecular dynamics sampling. Base exchange kinetic models are proposed that can accommodate observed differences between the inhibition mechanisms of these enzymes in terms of their physical properties, and kinetic estimates for these parameters are evaluated through computational modeling. These results establish foundations for quantitative modeling of NAD^+/NAM regulation of mammalian sirtuins during aging as well as criteria for the computational design of sirtuin activators that operate through alleviation of base exchange inhibition.

Author Summary

Sirtuins are in the spotlight because of their ability to protect against age-related diseases and to serve as key mediators of longevity in evolutionarily distant organismic models. As a product of the sirtuin deacetylation reaction, nicotinamide can inhibit sirtuin activity. A fundamental study of the mechanism of inhibition of SIRT3, the major mitochondrial sirtuin, by nicotinamide and related small molecules will establish a foundation for understanding the scope for physiological and artificial regulation of this enzyme. In this work, we applied computational modeling in conjunction with experimental kinetic assays in order to elucidate the mode of inhibition for SIRT3. Computational modeling and binding affinity estimation with SIRT3 in both the apo- and substrate-bound forms complement the kinetic data to reveal qualitative differences between the inhibition kinetics of SIRT3, SIRT1 and Sir2 that can be explained by appropriate inhibition kinetics models based on the sirtuin reaction mechanism. Kinetic estimates for these parameters are evaluated through computational modeling. Our results extend current understanding of SIRT3 biochemistry and may also guide the design of a new generation of SIRT3 modulators.

Introduction

Many severe diseases often occur later in life (e.g., diabetes, neurodegenerative diseases, cancer, cardiovascular disease, pro-inflammatory diseases, and osteoporosis), indicating that aging is an important risk factor for these conditions[1]. Sirtuins, the highly conserved homologues of the yeast Sir2 enzyme, have been implicated in aging and the regulation of metabolism and genome stability[2,3]. In mammals, seven sirtuin genes, SIRT1 to SIRT7, have been identified[4,5]. Human sirtuin type 3 (hereafter referred to as SIRT3 unless otherwise specified), one of the seven mammalian sirtuins thus far identified, is a major mitochondrial protein and has an NAD^+-dependent deacetylase activity regulating global mitochondrial lysine acetylation[6,7]. Proper mitochondrial function is required for metabolic homeostasis and involves careful regulation of the activity of multiple metabolic enzymes. SIRT3 targets many key metabolic enzymes, including Ac-CS2 (acetyl-CoA synthetase 2)[8,9], OTC (ornithine transcarbamylase)[10], LCAD (long-chain acyl-CoA dehydrogenase)[11], and ALDH2 (aldehyde dehydrogenase 2, therefore potentiating fat metabolism during fasting)[12]. In addition, SIRT3 destabilizes the hypoxia-inducible factor HIF-1α, which plays a central role in the Warburg reprogramming of mitochondria – a process that constitutes a critical step in tumorigenesis and aging [13,14].

Most sirtuins are NAD^+-dependent lysine deacylases, requiring the cofactor NAD^+ to cleave acyl groups from lysine side chains of their substrate proteins. Mammalian sirtuins have evolved NAD^+ binding affinities that are low enough that the enzyme activities can be effectively regulated by changes in the physiological concentrations of the cofactor (which according to some reports may range from 200 to 500 μM), allowing them to serve as NAD^+ sensors[15]. Decreases in NAD^+ levels that accompany organismic aging can downregulate sirtuin

activity[16,17], whereas increases in NAD^+ levels that occur due to caloric restriction or NAD^+ supplementation can upregulate sirtuin activity. Unlike allosteric activators like resveratrol, which are SIRT1-specific and have not been successfully applied to SIRT3[13], NAD^+ supplementation can activate most mammalian sirtuins. Indeed, recent reports have shown that NAD^+ supplementation through NAD^+ precursors like nicotinamide riboside (NR) or nicotinamide mononucleotide (NMN) can not only mitigate signs of aging but can in certain cases reverse them in some mammals through upregulation of sirtuin-dependent pathways[16,18,19]. Moreover, the sensitivity of mammalian sirtuin activity to NAD^+ levels is in fact the basis of circadian oscillations that regulate the 24 hour diurnal cycles of mammals[20].

Nicotinamide, a well-known water soluble sirtuin inhibitor, is the amide form of vitamin B3 (nicotinic acid), and acts as a constituent of the enzyme cofactors NAD^+(nicotinamide adenine dinucleotide) and NADP (nicotinamide adenine dinucleotide phosphate)[21]. NAM is a physiological negative regulator of human sirtuins and is a reaction product and endogenous inhibitor of the deacylation reaction. Physiological NAM levels in some mammals cells can lie in a range similar to the IC_{50}'s of several sirtuins[22-24], suggesting that sirtuins may also act as NAM sensors. Mechanistically, NAM binds to a conserved region in the sirtuin catalytic site and favors a base-exchange reaction instead of deacetylation[25]. An NAM analogue, isonicotinamide (isoNAM), which competes for free NAM binding but does not react appreciably with the enzyme intermediate, increases Sir2 activity[26].

Although all sirtuins undergo some level of base exchange inhibition by NAM, it has become increasingly clear that sirtuins have evolved diverse mechanisms for regulation by NAM that are suited to their physiological roles, just as they have evolved different mechanisms for regulation by NAD^+. For example, Sir2Af2 is only partially inhibited by NAM, whereas NAM

can completely inhibit mSIRT1[27]. hSIRT5 is a mammalian sirtuin that is only partially inhibited by NAM and largely insensitive to NAM at physiological concentrations[28]. mSIRT3 was reported to display apparent competitive inhibition by NAM, unlike the apparent noncompetitive inhibition reported for other sirtuins[29]. Quantitative understanding of the mechanism of inhibition by NAM is essential for predicting the effects of varying NAD^+/NAM levels on SIRT3 activity as well as for the rational design of activators that increase SIRT3 activity by alleviation of NAM inhibition. However, due to the sensitivity of NAM regulation kinetics to parameters including the binding affinities of NAD^+ and NAM, as well as the equilibrium constant for base exchange, the origins of the differences in NAM regulation of sirtuins remain poorly understood.

Available experimental evidence – such as x-ray structures and kinetic assays – is often limited in its ability to explain mechanistic details of sirtuin inhibition by NAM, isoNAM and other inhibitors; computational modeling can further elucidate the inhibitory mechanism. Thus far, crystallographic structural analysis of sirtuin binding sites has not been able to explain important differences in binding affinities between sirtuins that play a critical role in their physiological regulation. As will be seen below, evaluation of such binding modes is important for understanding the differences between the mechanisms by which inhibitors exert their effects on SIRT3 and other sirtuins. Computational modeling can evaluate the energetics and intermolecular interactions of binding modes – including unfavorable binding modes -- that are difficult to crystallize Such modeling can elucidate the energetic origins of binding affinity differences, which are often dynamic, more so than a single crystal structure, using methods like the Molecular Mechanics – Poisson Boltzmann (Generalized Born) Surface Area (MM-PB(GB)SA) technique[30-33]. While such binding affinity estimates do not typically provide

accurate absolute ΔG's of binding, they often display significant correlation with experimental binding affinities when used with high-resolution x-ray structures. Finally, the design of novel high affinity and specificity modulators can be aided by the computation of binding affinity estimates for docked ligands.

In this paper, the inhibition mode of NAM for SIRT3 is investigated and compared to that for SIRT1 and Sir2. First, experimental studies of the inhibition kinetics are reported. The mechanism of NAM as a SIRT3 inhibitor is then elucidated through computational studies, including induced fit docking, molecular dynamics simulations and binding affinity estimates of the NAM and the native NAD^+ cofactor for Sir2 and SIRT3. Important differences between the inhibition kinetics of SIRT3 and SIRT1 by NAM vis-à-vis the binding of NAD^+ are identified and explained through appropriate kinetic models. Furthermore, the prospects for molecules like isoNAM upregulating SIRT3 and SIRT1 activity are investigated. Our computational results support our experimental findings and provide a basis for the computational design of SIRT3-specific modulators.

Results

NAM Inhibition at Physiological Concentration

NAM is a known inhibitor of the deacetylation activity of sirtuins, but the inhibition mechanism of NAM has not yet been determined for human SIRT3. In order to compare the inhibitory potency of NAM toward SIRT3 to other human sirtuins, we measured its IC_{50} value-the concentration of inhibitor required to cause 50% inhibition under a given assay condition[34]. The inhibition of SIRT3 deacetylation by nicotinamide and isonicotinamide was tested in the presence of different concentrations of NAM and isoNAM with 90 minutes

incubation of 1mM NAD^+ at 37 ^oC, providing IC_{50} values of 36.7±1.3 μM and 13.8±0.5 mM, respectively. Their IC_{50} values for SIRT1 were also measured using the same method. In the case of this enzyme, the IC_{50} of NAM is 68.1±1.8 μM and of isoNAM is 12.2±0.3 mM (Figure 1). These values are in good agreement with reported data[35].

A

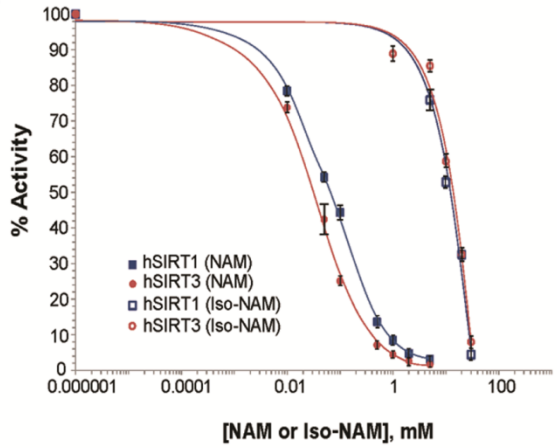

B

	IC50, μM	
	NAM	iso-NAM
hSIRT1	68.1±1.8	12200±317.1
hSIRT3	36.7±1.3	13800±478.6

Figure 1. Inhibition of SIRT3/SIRT1 by nicotinamide and its analog. (A) Nicotinamide / isonicotinamide inhibition assays showing percent change in deacetylation activity as a function of NAM/isoNAM concentration. Data for the SIRT1 enzyme are indicated with closed squares and a blue curve; data for the SIRT3 enzyme are indicated with filled circles and a red line. **(B)** The inset table lists the IC_{50}s of the two inhibitors for these enzymes.

NAM Acts as a Noncompetitive Inhibitor of Recombinant Human SIRT1 and a Mixed Noncompetitive Inhibitor of Recombinant Human SIRT3 *in vitro*.

To gain more insight into the effects of NAM on SIRT3 activity, the *in vitro* SIRT3 deacetylation activity was measured in the presence of varying amounts of NAM. We utilized a

novel deacetylation activity assay that generates a fluorescent signal upon deacetylation of a peptide substrate. When incubated with acetylated substrate and NAD^+, recombinant human SIRT3 gives a strong fluorescent signal 10-fold greater than no enzyme and no NAD^+ controls (data not shown). Using this assay, we tested the ability of nicotinamide to inhibit deacetylation in the presence of varying concentrations of NAD^+ and saturating concentrations of p53(379-382) peptide substrate. The *in vitro* SIRT1 deacetylation activity was first measured.

The following hyperbolic mixed inhibition initial rate model, derived using steady state assumptions on the various steps of the sirtuin reaction mechanism, can account for the inhibition mechanism of sirtuins wherein [*NAM*] engages in a base exchange reaction by reacting with the ADPR-peptidyl intermediate to regenerate NAD^+ and peptide:

$$\frac{v}{v_{max}} = \frac{[NAD^+] \cdot (1 + \frac{[NAM]}{K_1})}{K_{m,NAD^+} \cdot (1 + \frac{[NAM]}{K_2}) + [NAD^+] \cdot (1 + \frac{[NAM]}{\alpha K_2})} \qquad (1)$$

The relationships between $K_{m,NAD+}$, v_{max}, K_1, K_2, and $K_3 \equiv \alpha K_2$ and the rate constants of the sirtuin reaction mechanism are examined in the Discussion. The parameter estimates and associated double reciprocal plots ($1/v$ vs $1/[NAD^+]$) for global nonlinear fitting of this model to the initial rate data for SIRT3 and SIRT1 inhibition by NAM are provided in Table 1 and Fig. 2, respectively. In both cases, the K_1 was estimated to be sufficiently large that the $[NAM]/K_1$ term in (Eq. 1) could be omitted from the rate expression. Hence K_1 estimates are not included in Table 1.

Table 1. Model parameter estimates from global nonlinear fitting of mixed inhibition models for SIRT3 and SIRT1 inhibition by isoNAM (equation 2) and NAM (equation 1).

	Inhibitor	$K_{m,NAD+}$, μM	V_{max}, μM/min	$K_2(K_i)$	α
SIRT3	isoNAM	1402	27.83	(4623)	8.87E+18
	NAM	673.3	32.96	29.4	2.735
SIRT1	NAM	168.2	7.30	51.3	0.848

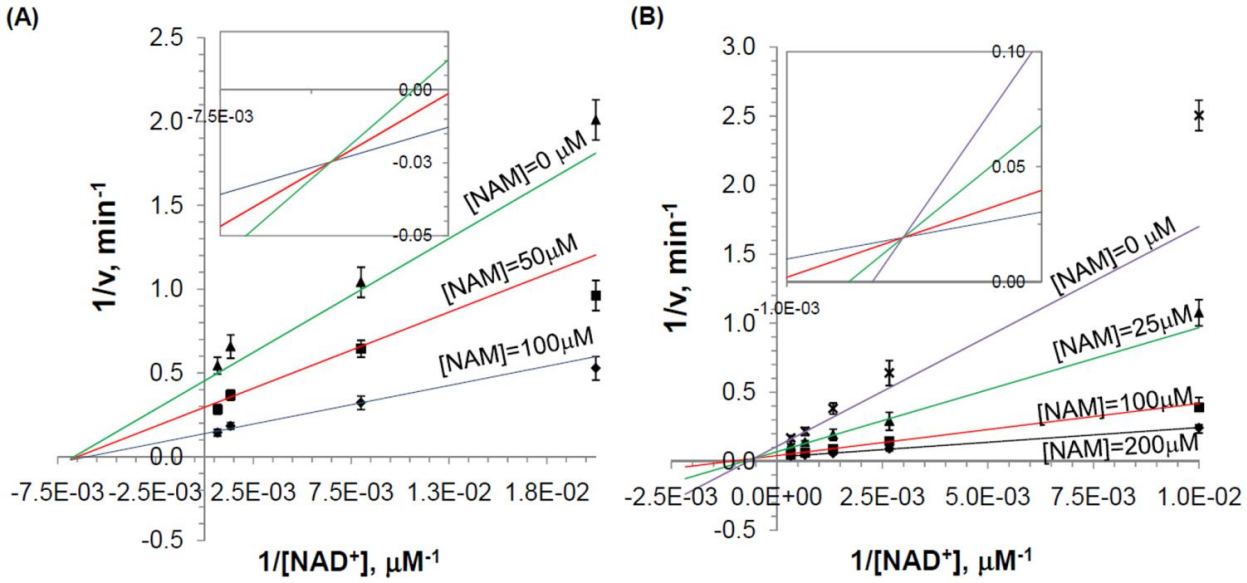

Figure 2. Inhibition of SIRT3/SIRT1 against NAD^+ by Nicotinamide. (**A**) Recombinant human SIRT1 was incubated for 0, 10, 20, 30, 60, 120, 180, and 240 min at 37°C in the presence of 50, 125, 750, 1500 μM NAD^+ and 0, 50, and 100 μM NAM. **(B)** Recombinant human SIRT3 was incubated for 0, 10, 20, 30, 60, 120, 180, and 240 min at 37°C in the presence of 100, 375, 750, 1500, 3000 μM NAD^+ and 0, 25, 100, and 200 μM NAM. Reactions were terminated by the addition of developer and samples were analyzed by fluorometry (excitation set at 355 nm and emission at 460 nm). Data are globally nonlinear fitted to base exchange inhibition model (Eq. 1) and shown as a double-reciprocal plot of arbitrary fluorescence units (AFU) min^{-1} versus $1/[NAD^+]$ μM^{-1}.

For SIRT1, a double reciprocal Lineweaver-Burk plot of the data (Figure 2A) shows that NAM displays approximately noncompetitive inhibition kinetics (see Discussion for definitions).

We next studied the inhibitory mechanism of nicotinamide in the case of SIRT3 *in vitro*. Using SIRT3, we monitored deacetylation of the substrate in the presence of varying amounts of NAM and NAD^+. Figure 2B reveals that NAM inhibition of SIRT3 is mixed noncompetitive with more apparent competition with respect to NAD^+ than inhibition of SIRT1. Figure 3 displays Dixon plots ($1/v$ vs $1/[NAM]$) for various $[NAD^+]$ for both SIRT1 and SIRT3.

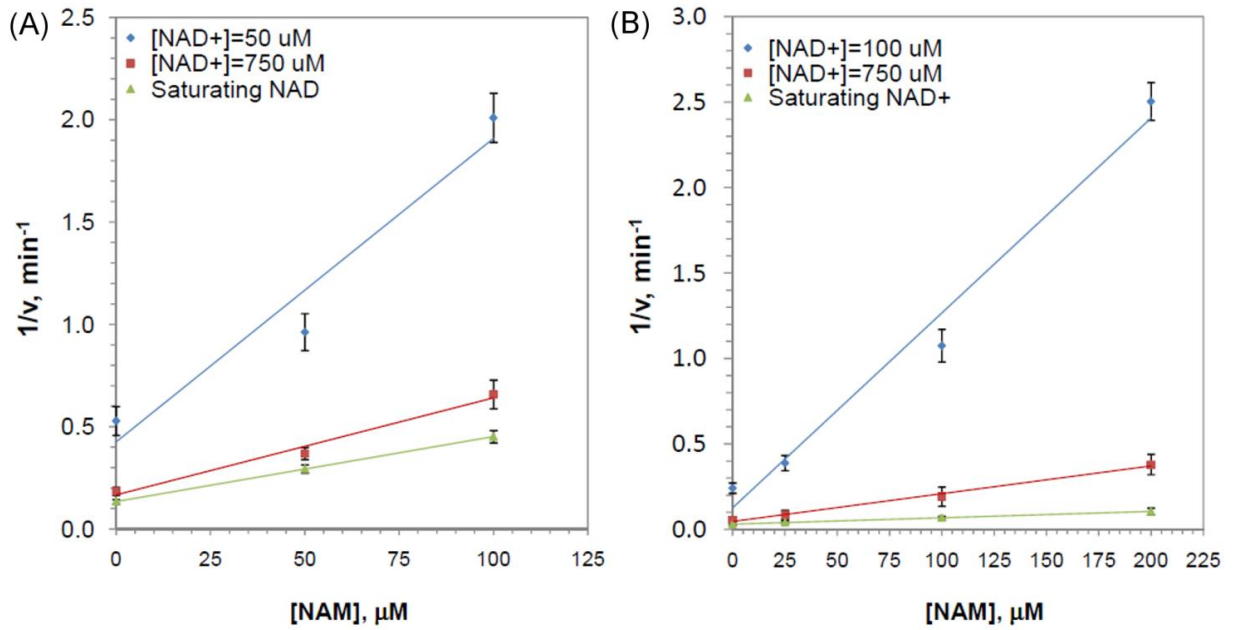

Figure 3. Deacetylation rate as a function of nicotinamide concentration. Dixon plot ($1/v$ vs $[NAM]$) of the deacetylation rates for **(A)** SIRT1 and **(B)** SIRT3 enzymes. Experimental data were fit to a linear equation.

IsoNAM Acts as a Competitive Inhibitor of hSIRT3 with respect to NAD^+ *in vitro*.

Isonicotinamide was reported as an activator of Sir2 activity [26] shown to directly compete with nicotinamide for binding. *in vivo* yeast studies indicated that Sir2-dependent silencing of the telomeric URA3 gene was upregulated by millimolar levels of isonicotinamide[36]. As a weak inhibitor of SIRT3, the effects of isoNAM on SIRT3 activity has not been investigated. Here, the *in vitro* SIRT3 deacetylation activity was measured in the presence of varying amounts of

isoNAM. Global nonlinear fitting of the following standard mixed noncompetitive inhibition model to initial rate data was carried out for isoNAM inhibition of SIRT3:

$$\frac{v}{v_{max}} = \frac{[NAD^+]}{K_{m,NAD^+} \cdot (1 + \frac{[I]}{K_i}) + [NAD^+] \cdot (1 + \frac{[I]}{\propto K_i})} \qquad (2)$$

where, [I] denotes the concentration of inhibitor (isoNAM). The definition of K_i in terms of the rate constants of the sirtuin reaction mechanism is provided in the Discussion.

The double reciprocal representation of the fitting is provided in Fig. 4, and associated parameter estimates are provided in Table 1. The high value of alpha indicates that isoNAM acts as a competitive inhibitor of SIRT3. Since the inhibition was observed to be competitive, and because of IC_{50} of isoNAM was orders of magnitude higher than that of NAM, the base exchange kinetic model (Eq. 1) was not fit.

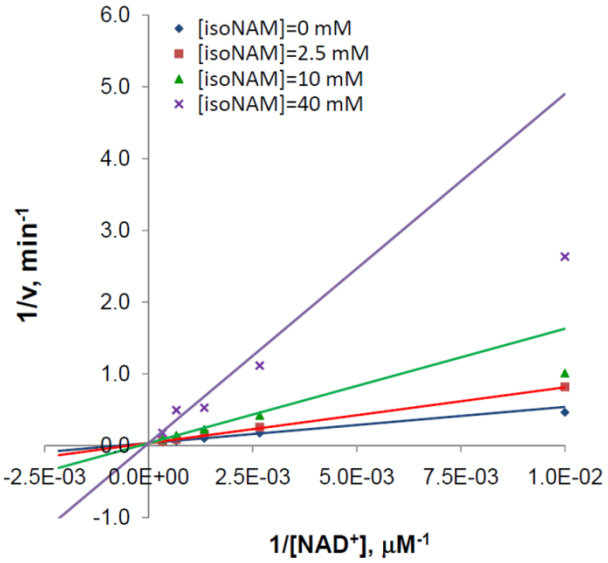

Figure 4. Inhibition of SIRT3 against NAD^+ by Isonicotinamide. Recombinant human SIRT3 was incubated for 0, 10, 20, 30, 60, 120, 180, and 240 min at 37°C in the presence of 100, 375, 750, 1500, 3000 µM NAD^+ and 0, 2.5, 10, and 40 mM isoNAM. Reactions were terminated by the addition of developer and samples were analyzed by fluorometry (excitation set at 355 nm and emission at 460 nm). Data are globally nonlinear fitted to mixed inhibition

model (Eq. 2) and shown as a double-reciprocal plot of arbitrary fluorescence units (AFU) min^{-1} versus $1/[NAD^+]$ μM^{-1}.

SIRT3 Inhibition Effect by NAM in the Presence of IsoNAM.

NAM is a potent inhibitor of the Sir2 reaction because of its ability to rebind with the enzyme and react with a high-energy intermediate, preventing deacetylation and regenerating starting materials [27,37]. In the case of some Sir2 enzymes, isoNAM, which does not readily react with the enzyme intermediate, was reported to relieve the inherent NAM inhibition by competitive binding. Prior reported work on isoNAM inhibition was restricted to Sir2 enzymes. Given the salient differences between mammalian and yeast sirtuins, we investigated whether this derepression effect of isoNAM also applies to SIRT3. The SIRT3 inhibition effect by NAM was studied in the presence of different concentrations of isoNAM. Figure 5 shows that in the presence of 100 uM NAM, sub-millimolar concentrations (50 - 900 μM) isoNAM slightly decreases the extent of SIRT3 inhibition by NAM – from 69.7% at 0 uM isoNAM to 56.5% at 900 uM isoNAM.

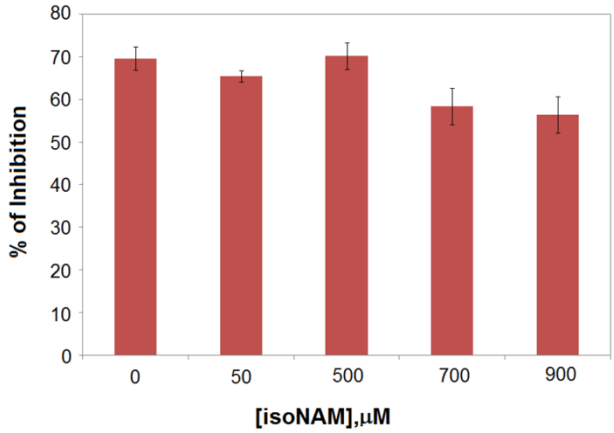

Figure 5. Inhibition of SIRT3/SIRT1 by nicotinamide in the presence of IsoNAM. Recombinant human SIRT3 was incubated with 50, 500, 700 and 900 μM of isoNAM for 40 min at 37°C in the presence of 500 μM NAD^+, and

100 μM NAM. Reactions were terminated by the addition of developer and samples were analyzed by fluorometry (excitation set at 355 nm and emission at 460 nm).

Computational Modeling of NAD^+ - Sir2 Binding

As a complement to the experimental studies, a computer simulation method involving molecular dynamics (MD) simulations of sirtuin complexes with NAD^+, NAM, and isoNAM as well as estimation of protein-ligand binding affinity with MM-PB(GB)SA scoring function evaluation was used, as described in Methods. MD simulations capture dynamic contributions to protein-ligand binding that are not apparent from single-structure calculations. MM-PB(GB)SA scoring functions, reported in kcal/mol, are not absolute binding affinities, but they have been shown to have a significant correlation with experimental binding affinities for many protein-ligand data sets[30-33]. The studies by Hou's group suggested that MM-PBSA performed better for absolute binding free energies and MM-GBSA had better correlation. Therefore results from both methods were presented.

Due to the aforementioned differences in NAD^+ and NAM regulation of yeast and mammalian sirtuins, we carried out computational studies of the above sirtuin-ligand complexes for bacterial Sir2Tm and hSIRT3. For both these enzymes, high-resolution crystal structures of their ternary complexes with peptide substrates and NAD^+ or NAD^+ analog have been solved. Binding of peptide to sirtuin active sites has been shown to induce domain motions (between Zn-binding domain and the Rossmann fold domain) that are essential to formation of the catalytically active NAD^+ binding pocket[38,39], but difficult to model without the use of long MD simulations. Hence, PDB structure 2H4F of the Sir2Tm:Ac-p53:NAD^+ (Ac-p53 is an 18-residue sequence of 372-KKGQSTSRHK- K[Ac]-LMFKTEG-389 that derived from C-terminal domain of the acetyl-cellular tumor antigen p53 peptide) complex was used, instead of other

available structures of Sir2 enzymes such as Sir2Af2 (which does not have crystal structure of peptide-bound ternary complexes), was used for computational studies of NAD^+ binding to Sir2 enzymes. Due to the lack of availability of a binary SIRT1:peptide complex, analogous computational studies on SIRT1 were not carried out (currently SIRT1 PDB structures are only available in 4I5I[40], 4IG9 and 4KXQ[41]).

Previous work [42] indicated that there are two possible binding sites for NAD^+ in Sir2 – the so-called AB and AC pockets. AC pocket binding is required for deacetylation[43]. In both binding modes, the ADP-ribose moiety resides in the A pocket. However, the nicotinamide moiety can reside in either the B pocket or C pocket. Early reports on Sir2 inhibition by NAM hypothesized that the apparent noncompetitive inhibition observed in kinetic experiments might be attributable to binding of NAD^+ in the unproductive AB mode in the presence of NAM, which binds in the C pocket, followed by a conformational rearrangement to the catalytically productive AC binding mode upon dissociation of NAM [44]. Hence we also studied the Sir2Tm:Ac-p53:NAD^+:NAM complex computationally.

MM-PB(GB)SA binding affinity estimates for NAD^+ and NAM in these complexes were computed by calculating substrate-receptor interaction energies from 20 ns MD trajectory for ternary complex and 27 ns MD trajectory for complex with NAM starting from the complex structures prepared as described in Methods. The MM-PB(GB)SA binding affinity estimates for NAD^+ in the AC and AB pockets were -23.19±7.27 (-105.48±6.48) kcal/mol and -16.15±8.35 (-81.78±8.01) kcal/mol, respectively (Tables 2 and 3). A breakdown of energetic contributions to NAD^+ binding is also provided in the tables. Fig. 6 compares the structural average of the last 10 ps of the MD trajectory (see Methods) to the co-crystallized structure of NAD^+ as in ternary complex structure of Sir2Tm (2H4F) by alignment of the A pocket. The RMSD of backbone of

these residues between crystal structure and MD averaged structure is 0.60 Å. The RMSD of NAD^+ itself (heavy atoms only) after alignment between crystal structure and MD averaged structure is 1.14 Å. Fig. 7 shows a close-up of NAD^+ adopting the AB binding mode in the presence of NAM.

Table 2.MD/MM-PB(GB)SA binding affinity estimates for NAD^+ in SIRT3:Ac-CS2:$NAD^+$and Sir2Tm:Ac-p53:NAD^+ in catalytically productive (without NAM) binding mode.

	SIRT3:Ac-CS2:NAD^+		Sir2Tm:Ac-p53:NAD^+	
	Average	Std. Dev.	Average	Std. Dev.
ΔVDWAALS	-68.85	4.82	-78.24	4.71
ΔEEL	-2.14	18.13	-142.87	11.80
ΔEGB	14.13	15.11	125.91	8.05
ΔESURF	-8.76	0.25	-10.28	0.16
ΔEPB	24.47	15.75	152.11	8.21
ΔENPOLAR	-46.14	1.10	-51.62	0.66
ΔEDISPER	87.31	1.58	97.43	0.98
ΔG_gas	-70.99	17.71	-221.11	11.07
ΔG_solv_igb2	5.36	15.11	115.64	8.02
ΔG_solv_pb	65.64	16.00	197.92	8.26
ΔG_igb2	**-65.63**	**5.91**	**-105.48**	**6.48**
ΔG_pb	**-5.35**	**8.37**	**-23.19**	**7.27**

VDWAALS: van der waals not including the 1-4 terms
EEL: electrostatic interactions not including the 1-4 terms
EGB: Polar contribution to solvation energy by GB method
ESURF: non-polar contribution to solvation energy using SASA (solvent accessible surface area) for GB
EPB: Polar contribution to solvation energy by PB method
ENPOLAR: non-polar contribution to solvation energy from repulsive solute-solvent interactions for PB
EDISPER: non-polar contribution to solvation energy from attractive solute-solvent interactions for PB
G_gas: Gas phase MM energy including all bonded and non-bonded terms
G_solv_igb2: Total solvation energy by GB method
G_solv_pb: Total solvation energy by PB method
ΔG_igb2: Difference in total energy including gas phase MM energy and solvation energy by GB method
ΔG_pb: Difference in total energy including gas phase MM energy and solvation energy by PB method

Table 3. MD/MM-PB(GB)SA binding affinity estimates for NAD^+ in SIRT3:Ac-CS2:NAD^+ and Sir2Tm:Ac-p53:NAD^+ in catalytically unproductive (with NAM) binding modes.

	SIRT3:Ac-CS2:NAD^+:NAM		Sir2Tm:Ac-p53:NAD^+:NAM	
	Average	Std. Dev.	Average	Std. Dev.
ΔVDWAALS	-72.94	4.35	-72.40	4.57
ΔEEL	52.57	13.53	-82.21	20.85
ΔEGB	-33.94	12.02	81.85	15.75
ΔESURF	-8.81	0.28	-9.03	0.33
ΔEPB	-27.80	12.52	96.05	18.91
ΔENPOLAR	-44.93	1.14	-47.08	1.44
ΔEDISPER	85.00	1.46	89.48	1.83
ΔG_gas	-20.37	13.27	-154.60	21.64
ΔG_solv_igb2	-42.76	12.10	72.82	15.62
ΔG_solv_pb	12.27	12.58	138.45	19.06
ΔG_igb2	**-63.12**	**4.37**	**-81.78**	**8.01**
ΔG_pb	**-8.10**	**5.71**	**-16.15**	**8.35**

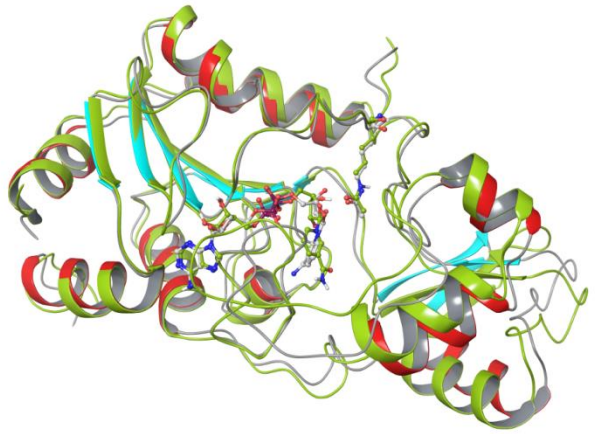

Figure 6. Alignment of ternary complex (Sir2Tm:Ac-p53:NAD^+) from MD averaged structure with respect to crystal structure. Ribbon representation of crystal structure (PDB ID: 2H4F) is colored by secondary structure (sheets in cyan, helixes in red and coils in gray), MD averaged structure (10 frames over last 10ps) in yellow green color. Carbon atoms in crystal structure are in white, and are in yellow green for MD averaged structure. Alignment was made using residues 15-27, 182-242, which forms the stable A binding pocket in Rossmann fold domain.

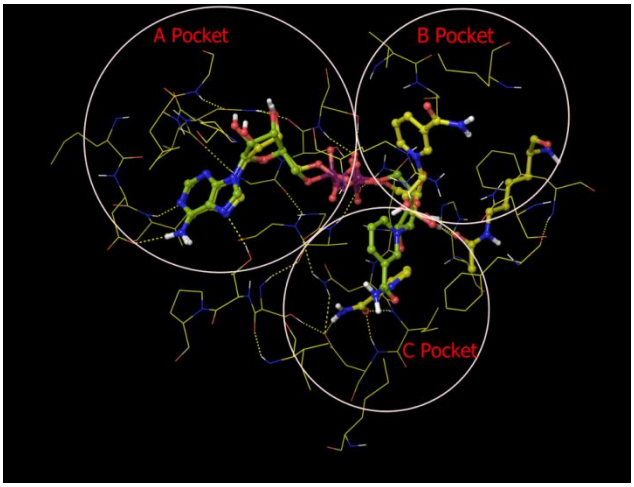

Figure 7. A B, and C pockets of the MD averaged structure of Sir2Tm complex with NAM (Sir2Tm:Ac-p53:NAD$^+$:NAM). Carbon is colored in yellow for MD averaged structure of 10 frames over last 10 ps, in yellow green for reference NAD$^+$ structure from MD averaged structure over last 10 ps of Sir2Tm ternary complex.

Computational Modeling of NAD$^+$ - SIRT3 Binding

Molecular dynamics simulations and MM-PB(GB)SA binding affinity calculations were also carried out for the SIRT3:NAD$^+$, SIRT3:Ac-CS2:NAD$^+$, and SIRT3:Ac-CS2:NAD$^+$:NAM complexes, where Ac-CS2 denotes a 12-residue sequence of 638-TRSG-K[Ac]-VMRRLLR-649 of acetyl-Co-A synthase 2, in order to investigate the structural and energetic origins of the aforementioned features of SIRT3 inhibition kinetics. As described in Methods, the starting structures for these simulations were based on PBD entry 4FVT, which is a ternary complex containing the unreactive NAD$^+$ analog carba-NAD$^+$ and Ac-CS2. In the case of the binary SIRT3:NAD$^+$ complex, the nicotinamide moiety and the Zn binding domain can move significantly over the course of MD when we align the Rossmann fold domain of SIRT3 (Supporting Information, Fig. S1). Binding affinity did not converge over 32 ns simulation. This is consistent with reports[39] that peptide binding is required to properly form the NAD$^+$ binding pocket in SIRT3.

The SIRT3:Ac-CS2:NAD^+ starting structure was prepared by converting carba-NAD^+ into NAD^+, whereas the SIRT3:Ac-CS2:NAD^+:NAM starting structure was prepared analogously to the Sir2Tm:Ac-p53:NAD^+:NAM complex, as described in Methods. Fig. 8 (a) compares the structural average of the last 10 ps of the MD trajectory for SIRT3:Ac-CS2:NAD^+ (where NAD^+ is in the catalytically productive binding mode) to the crystallographic coordinates of NAD^+ (from carba-NAD^+). The RMSD of NAD^+ (heavy atoms only) between crystal structure and MD averaged structure is 0.56 Å. Fig. 8(b) shows a close-up of NAD^+ adopting the catalytically unproductive binding mode in the presence of NAM. The NAD^+ in the quaternary complex including NAM is different from the AB pose observed in the crystal structure of Sir2Af2 in complex with NAD^+ and NAM (as in PDB structure 1YC2 chain A and D)[42]. Although the nicotinamide moiety has similar orientation in the two cases, the ribose connecting nicotinamide moiety moves closer to the C binding pocket in the SIRT3 quaternary complex with NAM, and the protein-ligand interactions also differ significantly. The MM-PB(GB)SA binding affinity estimate for NAD^+ in theSIRT3:Ac-CS2:NAD^+ complex is -5.35±8.37 (-65.63±5.91) kcal/mol whereas the binding affinity estimate for NAD^+ in SIRT3:Ac-CS2:NAD^+:NAM is -8.10±5.71 (-63.12±4.37) kcal/mol (Tables 2, 3). A breakdown of energetic contributions to NAD^+ binding is also provided in the tables.

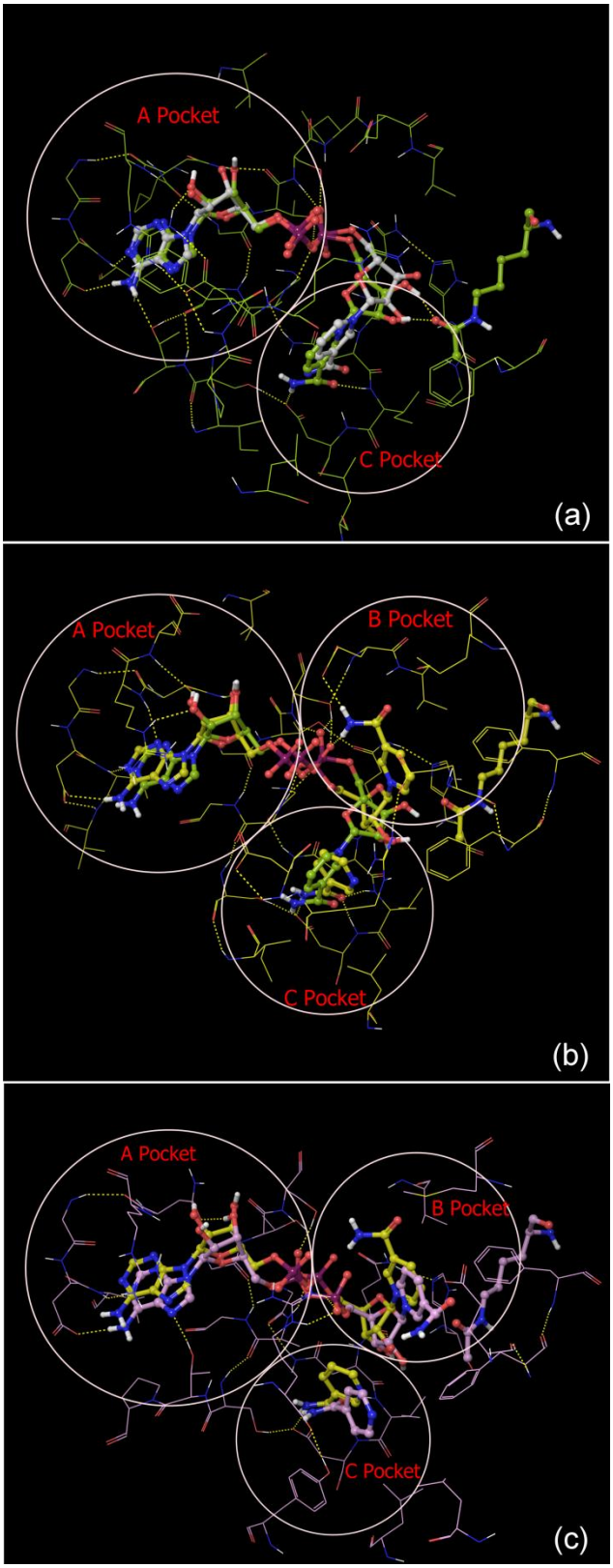
A Pocket
C Pocket
(a)
A Pocket
B Pocket
C Pocket
(b)
A Pocket
B Pocket
C Pocket
(c)

Figure 8. A, B and C binding pockets identified in MD averaged structure of different SIRT3 complexes. (a) A and C pockets from the MD averaged structure of 10 frames over last 10 ps of ternary complex (SIRT3:Ac-CS2:NAD^+, carbon in yellow green), reference NAD^+ structure (carbon in white) from crystal structure 4FVT; (b) A, B and C pockets from the MD averaged structure of 10 frames over last 10 ps of SIRT3 complex with NAM (SIRT3:Ac-ACS2:NAD^+:NAM, carbon in yellow), reference NAD^+ structure (carbon in yellow green) from MD averaged structure over last 10 ps of SIRT3 ternary complex; (c) A, B and C pockets from the MD averaged structure of 10 frames over last 10 ps of SIRT3 complex with isoNAM (SIRT3:Ac-ACS2:NAD^+:isoNAM, carbon in plum), reference NAD^+ structure (carbon in yellow) from MD averaged structure over last 10 ps of SIRT3 complex with NAM.

Computational Modeling of Nicotinamide/Isonicotinamide Binding to SIRT3 and Sir2

NAM and isoNAM bind in the conserved C pocket of sirtuins. In order to interrogate the possible role that NAM and isoNAM binding affinities may play in their mechanisms of their sirtuin inhibition, we carried out MM-PB(GB)SA binding affinity estimates for NAM and isoNAM in SIRT3 and for NAM in Sir2Tm. For NAM, the same MD trajectories reported above for SIRT3:Ac-CS2:NAD^+:NAM and Sir2Tm:Ac-p53:NAD^+:NAM were used. The SIRT3:Ac-CS2:NAD^+:isoNAM complex was prepared analogously to SIRT3:Ac-CS2:NAD^+:NAM. The MM-PB(GB)SA binding affinity estimates for NAM in SIRT3 and Sir2Tm were 0.26±3.26 (-19.82±1.89) kcal/mol and -5.78±3.51 (-29.74±2.05) kcal/mol, respectively (Table 4). A breakdown of energetic contributions to NAM and isoNAM binding in the AC pocket is also provided in the tables. Fig. 8(c) compares the structural average of the last 10 ps of the MD trajectories for the NAM and isoNAM complexes in SIRT3. The MM-GBSA calculations suggest that NAM binds slightly more strongly to the C pocket than isoNAM prior to enzymatic reaction (-19.82 kcal/mol vs -15.68 kcal/mol in MM-GBSA scores). While MM-PBSA calculations provide a more accurate representation of electrostatic contributions to solvation

free energies, MM-GBSA calculations have been reported to display higher correlations with experimentally measured binding free energies.

Table 4. MD/MM-PB(GB)SA binding affinity estimates for NAM and isoNAM in SIRT3:Ac-CS2:NAD^+ and Sir2Tm:Ac-p53:NAD^+

	SIRT3:Ac-CS2: NAD^+:NAM		Sir2Tm:Ac-p53: NAD^+:NAM		SIRT3:Ac-CS2: NAD^+:isoNAM	
	Average	Std. Dev.	Average	Std. Dev.	Average	Std. Dev.
ΔVDWAALS	-20.34	1.90	-19.94	1.87	-19.46	2.32
ΔEEL	-24.10	2.84	-18.48	2.95	-11.58	3.69
ΔEGB	27.51	1.64	20.57	1.69	18.10	2.02
ΔESURF	-2.89	0.08	-2.88	0.08	-2.75	0.16
ΔEPB	33.96	2.84	22.49	2.98	23.94	2.93
ΔENPOLAR	-14.47	0.25	-14.44	0.28	-13.49	0.59
ΔEDISPER	25.20	0.59	24.60	0.64	24.47	0.93
ΔG_gas	-44.44	2.59	-38.42	2.84	-31.04	3.67
ΔG_solv_igb2	24.62	1.63	17.69	1.67	15.35	2.01
ΔG_solv_pb	44.70	3.20	32.65	3.15	34.92	3.33
ΔG_igb2	**-19.82**	**1.89**	**-20.74**	**2.05**	**-15.68**	**2.48**
ΔG_pb	**0.26**	**3.26**	**-5.78**	**3.51**	**3.89**	**4.18**

Discussion

SIRT3 is a mitochondrial deacetylase protein that can regulate a number of cellular processes, including apoptosis, growth, and metabolism[45]. It has been reported that SIRT3 has tumor suppressive functions and reduces the glycolytic metabolism. Cancer initiation and progression depend on aerobic glycolysis, by which cancer cells synthesize biomass for their rapid growth[13].

For example, an important step in cancer initiation is so-called Warburg reprogramming, wherein mitochondria switch to glycolytic metabolism. Warburg reprogramming is induced by hypoxia inducible factors, including HIF-1α, which is destabilized by both SIRT1 and SIRT3[14,16]. Warburg reprogramming has also been shown to be an important step in

organismic decline with aging. Importantly, Warburg reprogramming can be reversed in some casea by NAD^+ supplementation through a pathway that involves sirtuin upregulation[16].

On the other hand, for normal tissue, downregulation of SIRT3 by NAM would increase glycolytic metabolism and allow cells in impacted tissues to survive longer, reducing long-term tissue damage. Understanding the properties of the inhibitory mechanism of SIRT3 will help elucidate the mechanism of SIRT3-mediated deacetylation and allow improvements in the design of selectivity and affinity of both inhibitors and activators [46].

In the so-called "NAD^+ world" picture of global metabolic regulation, the relative concentrations of NAD^+ and NAM in intracellular subcompartments – which can vary with age – play a central role in regulating mammalian metabolism through sirtuin-dependent pathways[47]. The average ratio of NAD^+ to NAM concentrations in a cellular subcompartment can decrease with age, due to factors including consumption of NAD^+ by the NAD^+-dependent PARP DNA repair enzymes[17] and reduced levels of NAD^+ synthesis from NAM by the Nampt biosynthetic pathway[47]. SIRT3 regulation by NAD^+ levels in mitochondria was shown to be a primary determinant of cellular resistance to apoptosis [48]. Mammalian sirtuin activities also undergo higher frequency fluctuations due to oscillations in NAD^+/NAM levels originating in circadian rhythms in the expression of the Nampt enzymes[49]. For example, oscillations of SIRT3 activity (induced by circadian oscillations of NAD^+ levels in mitochondria) are responsible for the periodic feeding cycles of mammals through the resulting oscillations in global mitochondrial activity[49].

Recent reports have underscored the diversity in the catalytic activity of mammalian sirtuins. Not only do they display diverse substrate selectivities[3,50], but mammalian sirtuins have also evolved diverse strategies for regulation by NAD^+ and NAM based on the relative magnitudes of

their binding affinities for these molecules as well as the values of their base exchange equilibrium constants[28]. Due to the interplay of effects of NAD^+ and NAM binding in sirtuin regulation, mechanistic modeling of inhibition is essential for prediction of the effects of varying NAD^+/NAM ratios on sirtuin activity.

NAM is the physiological sirtuin inhibitor. The IC_{50} values for nicotinamide inhibition of bacterial Sir2, yeast Sir2, mouse Sir2, SIRT1, SIRT2, SIRT3, and SIRT5 were 26, 120, 160, 50, 100, 36.7 μM, and 1.6 mM respectively[27,28,51,52]. Nuclear NAM levels have been estimated to be 10-150 μM[26], which most likely make NAM a sirtuin activity regulator *in vivo*. Sir2 thus appears to be affected by physiological NAM concentrations, assumed to be up to 0.1mM, and a role of NAM as an endogenous Sir2 regulator has been supported by *in vivo* studies in yeast, flies, and mammalian cells[15,53]. NAM inhibition and isoNAM activation of Sir2 deacetylase activity are achieved without directly affecting substrate binding[26]. Low levels of NAM have been measured in several rat tissues, probably as a result of its rapid utilization in the synthesis of NAD^+ and other pyridine nucleotides [54]. However, NAM concentrations as high as 300 μM have been reported in the brain of Tg2576 mice, providing evidence that NAM concentrations could be a factor regulating sirtuin activities in mammalian cells[55].

Due to their low K_m's for NAD^+, yeast and bacterial sirtuins may be less sensitive to regulation by NAD^+ concentration than are mammalian sirtuins[21, 49]. Hence increase in [NAD^+] above average physiological levels in a subcompartment can effectively "activate" mammalian sirtuins[18] but may not have apronounced effect on yeast/bacterial sirtuins. The physiological importance of SIRT3 regulation by NAD^+ and NAM, and the experimental observation that NAM inhibition of SIRT3 is more competitive toward NAD^+ than inhibition of SIRT1, motivate a detailed study of the inhibitory mechanism of SIRT3.

Mode of Inhibition of SIRT3 by Nicotinamide

A common model used to fit enzyme inhibition kinetics is mixed noncompetitive inhibition [56]. In the case of sirtuin enzymes, in the presence of saturating peptide and varying NAD^+ substrate concentrations, mixed noncompetitive inhibition of deacetylation can be described according to equation (2). Mechanistically, mixed noncompetitive inhibition with nonzero $1/\alpha$ can originate through a) the inhibitor binding to both the free enzyme and enzyme-substrate complex (in the case that the inhibitor inhibits the forward reaction), b) promotion of the reverse reaction via binding of a reaction product to the enzyme or an enzyme-intermediate complex, or c) a combination of both. If $\alpha >> 1$ mixed noncompetitive inhibition becomes competitive inhibition. Here, the apparent K_m of the substrate is changed by the inhibitor, but the v_{max} is not. If $\alpha = 1$, the inhibition mode is said to be noncompetitive. In this case, the apparent K_m is not altered by the inhibitor, but v_{max} is. If $\alpha << 1$, the inhibition mode is called uncompetitive, and both K_m and v_{max} change by the same amount.

Unreactive C pocket-binding ligands like isoNAM exert their effect physically by binding to the enzyme and/or enzyme-substrate complex (here, we are concerned with the substrate NAD^+; and hence acetylated peptide is present in saturating concentrations). If the binding affinity for the free enzyme is substantially greater than that for the enzyme-substrate complex, the inhibition kinetics is competitive. In this case, $1/\alpha \approx 0$ in equation (2). If the K_d's for binding of the inhibitor to enzyme and enzyme-substrate complex are similar in magnitude, the inhibition is noncompetitive and mixed noncompetitive if the K_d's differ, according to equation (2) with $K_i = K_d$.

In the case of NAM, product inhibition can occur through promotion of a base exchange reaction with the reaction intermediate. A few groups have reported that NAM can react to regenerate acetyl-lysine and NAD^+ in a nicotinamide exchange reaction, in which the imidate intermediate is emptied during normal steady-state turnover, directing NAM inhibition of deacetylation [27,42,51]. It has been observed that NAM inhibition of Sir2 depends on its ability to condense with the high-energy enzyme:ADP-Ribose:acetyl-lysine intermediate to reverse the reaction, reforming NAD^+. Rebinding of NAM to the Sir2/intermediate complex can promote the reverse reaction to reform the substrates, thus inhibiting the deacetylation reaction [15]. By using [carbonyl-^{14}C] NAM, the base exchange reaction for Sir2 was extensively studied (Fig. 9).

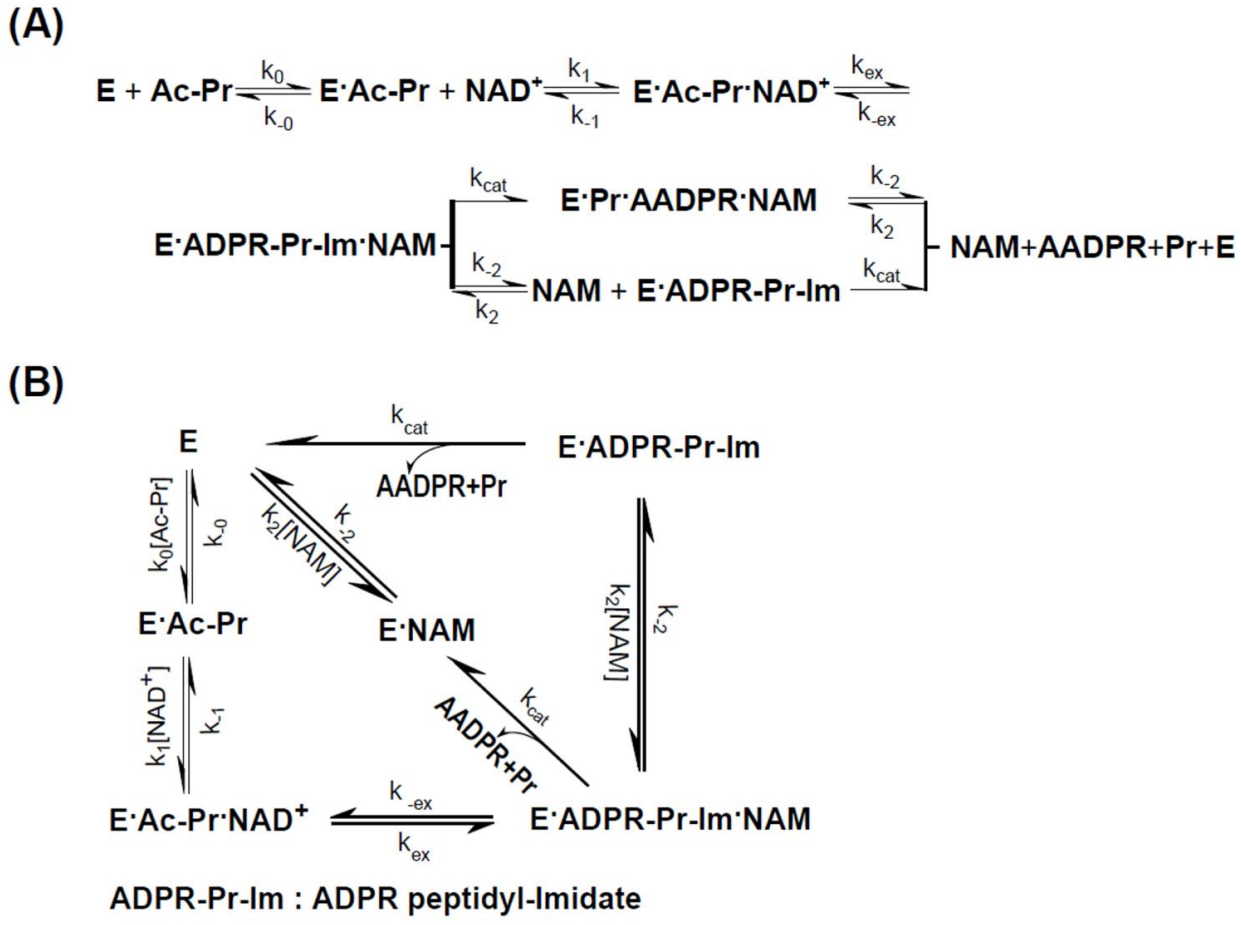

Figure 9. General model for the inhibition of sirtuins by NAM. (A) Reaction scheme for the sirtuin deacetylation reaction and base exchange inhibition. For simplicity, deacetylation and AADPR + Pr dissociation are assumed to occur together (k_{cat} denotes the rate constant for deacetylation and dissociation of AADPR + Pr from E). **(B)** Simplified reaction network for base exchange inhibition. In the presence of saturating Ac-Pr, E is rapidly converted into E·Ac-Pr and NAM binding to E can be neglected, resulting in a simplified reaction network with 5 species. ADPR, adenosine diphosphate ribose; AADPR, O-acetyl-adenosine-diphosphate-ribose.

Competition between nicotinamide exchange and deacetylation reactions occurs when NAM is present. This competition partitions the intermediate forward (a α-face nucleophilic process) and backward (β-face nucleophile process) to provide inhibition of deacetylation. An intermediate-forming step is involved into both exchange and deacetylation reactions, and the ratio is determined by the rates of the chemical processes.

An initial rate model for NAM base exchange inhibition was provided in equation (1). Analysis of the sirtuin reaction scheme, shown in Fig. 9, is necessary for derivation of the explicit expressions for the inhibition constants in this equation.

Fig. 9 depicts acetylated peptide binding occurring prior to NAD^+ binding in an ordered bireactants model. This is supported by the SIRT3:NAD^+ binary complex molecular dynamics data (Fig S1), which shows very weak binding to SIRT3 and highly dynamic fluctuations of the nicotinamide moiety of the ligand in the absence of peptide. Under saturating peptide concentrations, nearly all E is converted rapidly to E·Ac-Pr, and hence both E and the step E→E·NAM can also be omitted from the reaction scheme. The catalytic chemistry following the formation of the ADPR-Pr-Im(alkylimidate) intermediate has been modeled using mixed quantum/molecular mechanics (QM/MM) simulations in non-mammalian sirtuins [57]. k_{cat} in our model can be interpreted as the rate constant of the rate limiting step of this catalytic chemistry

and the dissociation of AADPR+Pr (which for simplicity is assumed to occur concurrently with deacetylation).

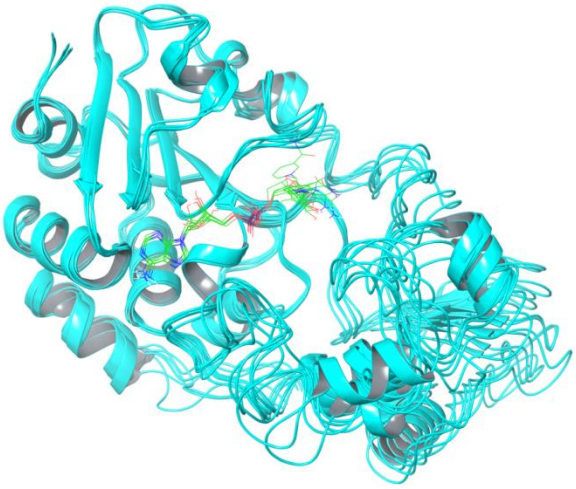

Figure S1. Snapshots taken from MD simulations of SIRT3:NAD$^+$ binary complex. Averaged structures of 10 frames over 10 ps at 22, 24, 26, 28, 30 and 32 ns from MD simulation of binary complex (SIRT3:NAD$^+$). Alignment was made using residues 139-151, 313-378 in Rossmann fold domain that forms A binding pocket with respect to SIRT3 ternary complex crystal structure 4FVT.

For base exchange inhibition by NAM, applying a steady-state analysis to the reaction scheme in Fig. 9B results in the initial rate model (1), where $K_{m,NAD+}$, K_1, K_2, and $K_3 \equiv \alpha K_2$ are functions of the rate constants in the Figure that can be obtained by solution of the linear system of algebraic steady state conditions and mass balance constraints. A full analysis will be reported in a separate work. Under the approximation where $k_{cat} << k_j$, $j \neq cat$, we find

$$\frac{v}{v_{max}} \approx \frac{[NAD^+] \cdot (1 + \frac{[NAM]}{K_{d,NAM}})}{K_{m,NAD^+} \cdot (1 + \frac{K_{d,NAD^+} \cdot K_{ex}}{K_{m,NAD^+} \cdot K_{d,NAM}}[NAM]) + [NAD^+] \cdot (1 + \frac{1+K_{ex}}{K_{d,NAM}}[NAM])} \qquad (3)$$

where $K_{d,NAM} = \frac{[E \cdot ADPR \cdot Pr-Im] \cdot [NAM]}{[E \cdot ADPR \cdot Pr-Im \cdot NAM]}$. We do not explore the accuracy of this approximation in the present work. For sirtuins, $k_{cat} << k_j,\ j \neq cat$ does not imply $K_{m,NAD+} \approx K_{d,\ NAD+}$. We do not explore the accuracy of this approximation in the present work.

Due to the diagonal path in Fig. 9B (equivalently, the upper branch in Fig 9A), base exchange inhibition for sirtuins can be hyperbolic mixed inhibition [56] where the inhibitor affects the numerator of the initial rate expression, since deacetylation can occur from both NAM-bound and dissociated complexes. The fact that the NAM-bound complex is catalytically active results in a plateau in $1/v_{max}$ at saturating $[NAD^+]$. The maximum possible extent of base exchange product inhibition can be found as follows.

$$\frac{1}{v} = \frac{1 + \frac{[NAM]}{K_1}}{v_{max} \cdot (1 + \frac{[NAM]}{K_{21}})} = \frac{K_3 + [NAM]}{v_{max} \cdot (K_3 + \frac{K_3}{K_1}[NAM])} \qquad (4)$$

The remaining activity as a fraction of maximal rate (v_{max}) in absence of inhibitor at saturating $[NAD^+]$ is thus given by $K_3/K_1 \approx 1/(1+K_{ex})$ where the approximate equality holds in the case that $k_{cat} << k_j,\ j \neq cat$. The Dixon plots in Fig. 4 show that $K_{ex} >> 1$ for both SIRT3 and SIRT1 Initial rate data at higher $[NAM]$ (not reported here) can be used to obtain a better estimate of K_1 and K_{ex}.

Since SIRT3 and SIRT1 are both nearly completely inhibited by NAM, this implies $K_1 >> K_3$, which was confirmed by the results (Table 1) of global nonlinear fitting of (1) for these enzymes. Due to the large value of K_{ex} and hence K_1 it can be shown that at sufficiently low $[NAM]$ the plots of $1/v$ vs $1/[NAD^+]$ at various $[NAM]$ intersect at a single point, at

$$\frac{1}{[NAD^+]_{int}} = -\frac{K_2}{K_{m,NAD^+}} \cdot \frac{1}{K_3} = -\frac{1}{\alpha K_{m,NAD^+}} \approx -\frac{1}{K_{d,NAD^+}} \cdot \frac{1 + K_{ex}}{K_{ex}} \qquad (5)$$

with

$$\alpha = \frac{K_3}{K_2} \approx \frac{K_{d,NAD^+}}{K_{m,NAD^+}} \cdot \frac{K_{ex}}{1 + K_{ex}} \qquad (6)$$

where the approximate equalities again refer to the case $k_{cat} << k_j$, $j \neq cat$. Fig. 10 graphically depicts the definition of α for base exchange inhibition.

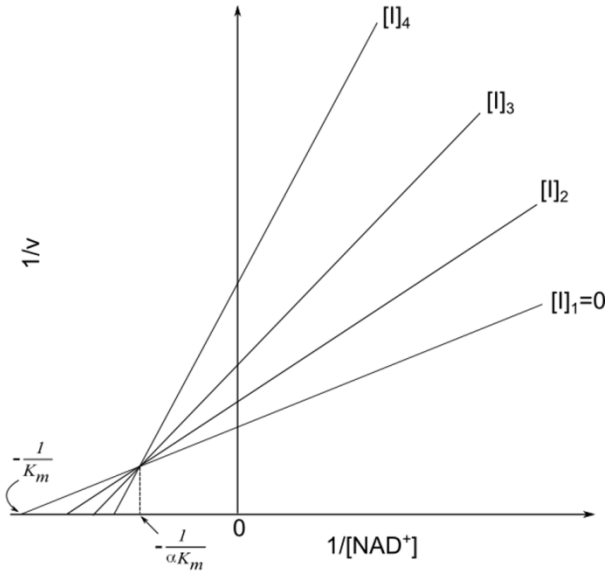

$$\alpha = \frac{K_3}{K_2} \approx \frac{K_{d,NAD^+}}{K_{m,NAD^+}} \cdot \frac{K_{ex}}{1+K_{ex}}$$

Figure 10. Mixed noncompetitive base exchange inhibition kinetics of sirtuin enzymes: mechanistic interpretation.

Hence a higher ratio of the dissociation constant for NAD^+ to the Michaelis constant for NAD^+ is expected to result in a higher value of α, as is observed with SIRT3 (Table 1). Based on this analysis, we see how physical properties of a sirtuin affect its value of α. The greater competitive behavior in the inhibition kinetics of SIRT3 is also visible in the Dixon plots of Fig. 4; more competitive behavior leads to a smaller slope of $1/v_{max}$ vs $[NAM]$. Note that equation (6) is not intended to provide an accurate estimate of $K_{d,NAD+}$, due to the aforementioned approximations.

On the other hand, if inhibition were primarily caused by binding of inhibitor to enzyme and enzyme-substrate complexes, thereby inhibiting the forward reaction – i.e., if K_d of an inhibitor I referred to the dissociation constant $\frac{[E\cdot Ac-Pr]\cdot[I]}{[E\cdot Ac-Pr\cdot I]} = \frac{[E\cdot Ac-Pr\cdot NAD^+]\cdot[I]}{[E\cdot Ac-Pr\cdot NAD^+\cdot I]}$ mixed noncompetitive inhibition could still be observed, but only base exchange product inhibition can amplify the effect of the inhibitor binding through K_{ex}, as shown in equation (3). If the concentrations of substrate and product are of the same order of magnitude (as they often are in physiological regulation of sirtuins), but the K_d of product is of a larger order of magnitude, potent inhibition requires reverse rate constants (for sirtuins, k_{-ex}) to be suitably large. Through appropriate values of $K_{m,NAD+}$, $K_{d,NAD+}$, K_{ex} , NAM inhibition of sirtuin enzymes can thus exhibit a range of potent mixed noncompetitive inhibition behavior. In particular SIRT3's may exhibit NAM base exchange inhibition kinetics that is apparently more competitive than that of SIRT1 due to a higher ratio $\frac{K_{d,NAD^+}}{K_{m,NAD^+}}$. Jin et al. observed $\alpha >> 1$ for mouse SIRT3 inhibition by NAM [39].

Several lines of evidence support this mechanistic model.-Most importantly, as in the case of SIRT3 (Table 1), prior reports of K_2 and αK_2 for Sir2 enzymes were similar in order of magnitude to $K_{m,NAD+}$, suggesting that they should not be interpreted as $K_{d,NAM}$ [28,37,58]. However, the above work did not explore the physical origins of the differences in the values of α for various sirtuins. Moreover, Jin et al. indicated that NAM inhibition of mSIRT3 may occur through a mechanism different from that of SIRT1 and Sir2, due to its more highly competitive nature. There are few if any direct measurements of $K_{d,NAM}$ for sirtuins, and to our knowledge, no structural energetic analysis analyzing the causes of the often substantially different values of α observed among sirtuins. Hence we undertook a detailed computational analysis of the energetics of the binding affinities of various complexes in the sirtuinreaction mechanism, as well as

complexes involving isoNAM, in order to critically evaluate various hypotheses regarding the origin of the greater competitive behavior in the inhibition kinetics of SIRT3 by NAM.

To date, computational modeling of sirtuin catalytic mechanisms has focused on mixed quantum/molecular mechanics simulations of reactive chemistry in non-mammalian sirtuins [59,60]. However, sirtuin regulation by NAD^+/NAM in mammals is heavily dependent on the enzyme's binding affinity for these molecules. To our knowledge, there have been no reports of computational studies of sirtuin inhibition by NAM addressing the critical binding events in the reaction mechanism.

Comparison of NAD^+ Binding Affinities in Catalytically Productive and Unproductive Binding Modes

As indicated above, there are two possible explanations of the greater degree of apparent competition between NAM and NAD^+ in the inhibition kinetics of hSIRT3/mSIRT3, compared to that of SIRT1. These are a) direct competition (reducing the rate of the forward reaction) and b) base exchange (increasing the rate of the reverse reaction). We consider the former scenario first.

Models for inhibition of the forward deacetylation reaction by NAM that can accommodate the possibility of mixed noncompetitive inhibition kinetics have been proposed previously[44]. These involve NAD^+ binding in the catalytically unproductive AB mode in the presence of NAM, with the nicotinamide moiety undergoing a rapid conformational shift to the C pocket upon the dissociation of NAM. Noncompetitive inhibition could occur in this model if the binding affinities of NAD^+ to the AB and AC pockets were the same. Mixed noncompetitive inhibition could occur within the model if the binding affinity of NAD^+ for the AC pocket were

somewhat lower or higher than its binding affinity for the AB pocket. If NAD^+ binds only to the AC pocket of a sirtuin, the model could produce competitive inhibition.

A necessary condition for this mechanism to be a possible explanation for the differences in observed sirtuin inhibition kinetics is thus that NAD^+ must bind with high affinity to the catalytically inactive (AB) site in SIRT1 and Sir2, concurrently with NAM binding. Hence the hypothesis can be investigated with computation.

Figs. 6 and 7 depict the structural averages of the last 10 ps of the MD trajectories for the Sir2Tm:Ac-CS2:NAD^+ (catalytically productive) and Sir2Tm:Ac-CS2:NAD^+:NAM (catalytically unproductive) complexes, respectively. The corresponding MD structural averages for SIRT3 are shown in Fig. 8(a) and (b). Neither the Sir2Tm or SIRT3 catalytically unproductive binding modes shown in these Figures have been identified crystallographically in the presence of bound peptide [25,42]. Comparison of the MM-GB(PB)SA binding affinity estimates for these complexes in Tables 3 and 4 reveals that in Sir2Tm, the catalytically unproductive binding mode is predicted to be less stable than the productive binding mode (-81.78 ±8.01 kcal/mol vs -105.48 ± 6.48 kcal/mol MM-GBSA, respectively). Moreover, in SIRT3, the estimated binding affinity of NAD^+ for the AB pocket (-63.12 kcal/mol MM-GBSA) is similar to that for the AC pocket (-65.63 kcal/mol). Hence, the simulations do not provide evidence for the proposed mechanism. Finally, the difference between the estimated binding affinities of the unproductive binding modes in SIRT3 and Sir2Tm is smaller than the difference in estimated binding affinities for the productive binding modes in these enzymes (Tables 3 and 4). Hence, the effect of the difference in $K_{d,NAD+}$'s for the catalytically active binding modes of these two enzymes may be more relevant to the inhibition mechanism, and will be discussed further below.

Comparison of NAM and isoNAM C Pocket Interactions

Another necessary condition for NAM inhibition to substantially decrease in the forward rate of the deacetylation reaction is that NAM must bind with affinity similar to that of NAD^+ (given that its IC_{50} is similar or smaller in magnitude than $K_{m,NAD+}$). Hence we sought to estimate the K_d of NAM, through the use of computational binding affinity estimates for NAM and isoNAM together with experimental estimates of $K_{d,isoNAM}$ for its structural isomer isoNAM.

Defining the inhibition modality is necessary for calculating the enzyme-inhibitor dissociation constant from the experimental assays [61]. For isoNAM inhibition, $\alpha >> 1$ and $K_i \approx$ 4.6mM – much higher than that of NAM (~ 50 μM) – were observed (Table 1), indicating that isoNAM inhibition does not occur through base exchange inhibition but rather through traditional competitive inhibition; i.e., isoNAM directly competes with NAD^+ for binding to SIRT3, and the unproductive NAD^+ binding mode depicted in Fig. 9 is unlikely to be part of the catalytic pathway. Prior literature[27] has indicated that isoNAM is not a base exchange substrate. This allows us to estimate K_d for isoNAM using its K_i obtained from fitting of equation (2).

Using the K_i for isoNAM reported in Table 1 as an estimate of $K_{d,isoNAM}$ for SIRT3, the corresponding protein-inhibitor Gibbs free energy of binding may be estimated using $\Delta G_{bind} = RTln(K_{d,isoNAM}) \approx$-*3.2* kcal/mol. Note this is not intended to be an accurate estimate of $K_{d,isoNAM}$, due to the approximations applied, but rather only its order of magnitude for the purpose of mechanistic analysis. Kinetic model for isoNAM inhibition is under development and more accurate estimation of isoNAM K_d, ΔG will be considered in future work.

Fig. 8(a) compares the binding modes of NAM and isoNAM in SIRT3 from MD simulations. Interaction diagrams in Figure 11 depict the relevant contacts between C pocket

residues and these ligands. Note that both NAM and isoNAM engage in favorable hydrogen bonding interactions through their amide groups with the side chain of Asp231 and backbone of Ile230. Similar hydrogen bonding interactions are observed in Sir2Tm:NAM (Figure S2). The MM-PB(GB)SA binding affinity estimates are slightly more favorable for NAM compared to isoNAM (-19.82 ± 1.89 kcal/mol vs -15.68 ± 2.48 kcal/mol MM-GBSA, respectively), but the difference lies within the standard errors of the MM-GBSA estimates. By comparison, in the presence of NAM, the nicotinamide moiety of NAD^+ in SIRT3 and Sir2Tm does not engage in both these hydrogen bonding interactions in the MD averaged structures (Fig. 8(a) and 7). The B pocket is more solvent-exposed, and contains fewer potential hydrogen bonding partners than the C pocket in SIRT3 and Sir2Tm. In the absence of peptide substrate, the nicotinamide moiety of NAD^+ can adopt a variety of conformations, some within the B pocket, in Sir2Tm[42] and in SIRT3 (see the MD trajectories depicted in Fig. S1). Upon peptide binding, domain motions induce formation of the NAD^+ binding pocket[38], rendering the C pocket conformation of the nicotinamide moiety more favorable. These observations indicate that any inhibition of the forward deacetylation reaction by NAM should be reduced further in potency below that predicted on the basis of its K_d alone, due to the energetically unfavorable effect of forcing the nicotinamide moiety of NAD^+ into the B pocket.

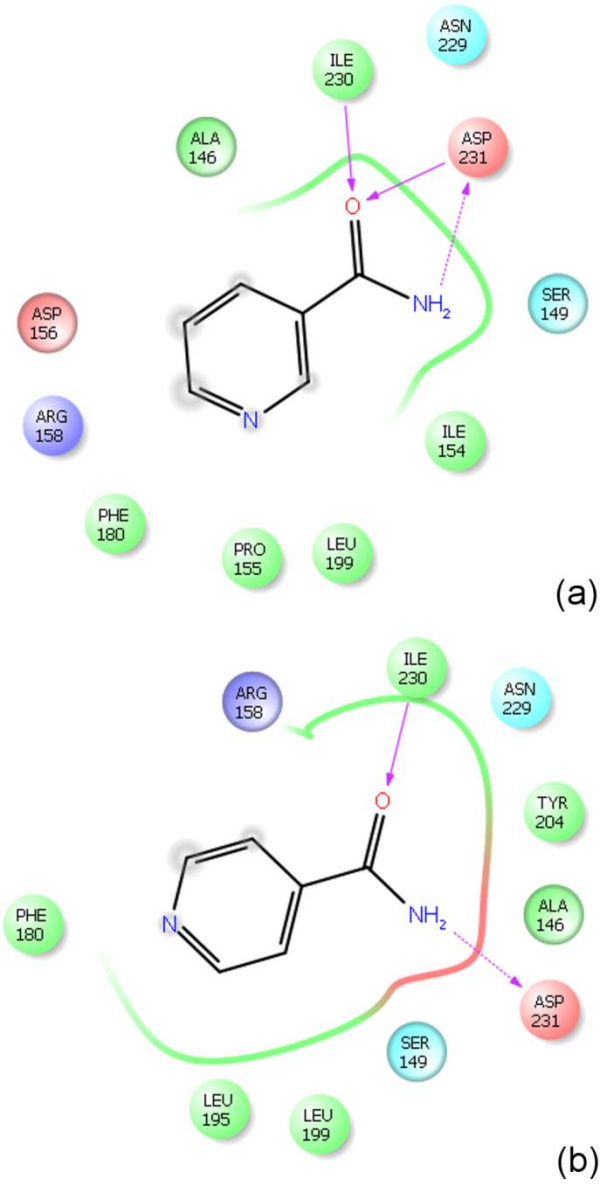

Figure 11. NAM/isoNAM interaction diagrams of MD averaged structures. (10 frames from last 10ps) (a) SIRT3 complex with NAM; (b) SIRT3 complex with isoNAM.

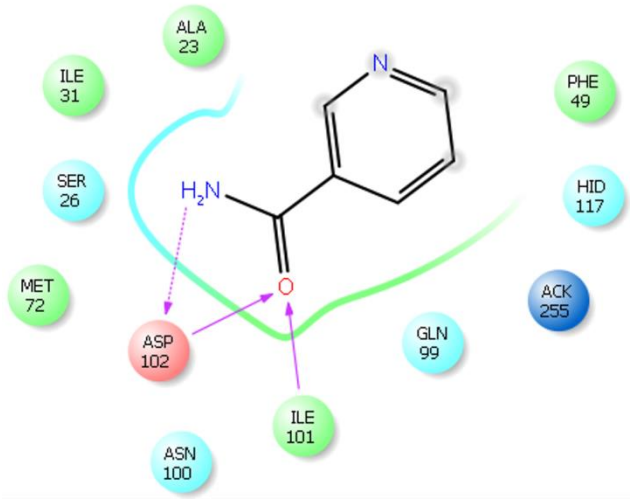

Figure S2. NAM interaction diagrams of MD averaged structures (10 frames from last 10ps) of Sir2TM complex with NAM.

Since MM-GBSA estimates can generally be used to rank order binding affinities [62], and since the difference of MM-GBSA binding affinity estimates for NAM and isoNAM is close to the standard errors of the estimates, we adopt $K_{d,isoNAM}$ as an upper bound for $K_{d,NAM}$. Applying the $k_{cat} << k_j,\ j \neq cat$ approximation for $K_3 \approx \frac{K_{d,NAM}}{1+K_{ex}}$, this also provides an approximate upper bound on the value of K_{ex} for SIRT3:

$$K_{ex} \approx \frac{K_{d,NAM}}{K_3} - 1 \leq \frac{4623}{51.3} = 86$$

which is consistent with the shape of the Dixon plots in Fig. 4. Again, we note that the approximation here is based on the assumption $k_{cat} << k_j,\ j \neq cat$, the accuracy of which is not considered in the present work. More accurate binding affinity estimates of NAM can also be made using linear interaction methods applied to a congeneric series[63] of C pocket binding ligands.

Effect of Energetics of NAD^+ Binding to SIRT3 on NAM Inhibition Kinetics

In the previous section we showed that computational binding affinity estimates predict that the K_d of NAM for SIRT3 is of the same order of magnitude as that of isoNAM. Since the IC50 of isoNAM is at least two orders of magnitude higher, product inhibition of SIRT3 by NAM at physiological concentrations should occur primarily through promotion of the reverse reaction. The value of α for SIRT3 provides further information regarding the relative magnitudes of binding rate constants and other (e.g., reverse) rate constants in the reaction mechanism through expression (6) relating $K_{d,NAD+}$, $K_{m,NAD+}$, and K_{ex}.

Consistently, comparison of the computationally estimated binding affinities of NAD^+ and NAM to SIRT3 in Tables 2 and 3, respectively, show that NAD^+ binds to SIRT3 substantially more strongly than does NAM. This can be attributed to the fact that the majority of favorable contacts with NAD^+ occur with ADPR moiety in the A pocket, including hydrogen bonding interactions between Ser321, Thr320 and the phosphate groups, as well as Asn244 and Arg345 to the ribose hydroxyl groups.

We therefore consider the hypothesis that base exchange inhibition is responsible for the greater degree of apparent competition in the NAM inhibition kinetics of SIRT3, using equation (6) and the reaction scheme in Fig. 11, since the effects of NAM binding to any enzyme species other than the alkylimidate intermediate can be neglected at physiological concentrations.

Equation (6) indicates that under the approximation $k_{cat} << k_j,\ j \neq cat$, α depends on $K_{d,NAD+}$, with more competitive character (greater α) corresponding to a higher ratio $\frac{K_{d,NAD^+}}{K_{m,NAD^+}}$ (note that $K_{m,NAD+}$ is also a function of $K_{d,NAD+}$). The energetics of binding of NAD^+ to the catalytically

productive AC pocket in Sir2 and SIRT3 can be compared computationally. The MM-PB(GB)SA binding affinity estimates in Table 2 are consistent with a significantly higher $K_{d,NAD+}$ for SIRT3.

Following features contribute to the significantly higher K_d, NAD^+ for SIRT3: Comparing the breakdown of binding energy contributions for SIRT3 and Sir2Tm in Table 2, the MD averaged structures in Fig. 7, 8(a) and the ligand interaction diagrams in Fig. 12, we see that NAD^+ has stronger binding affinity (-105.48 ±6.48 vs -65.63 ±5.91 kcal/mol by MM-GBSA) for Sir2Tm in the ternary structure. The main contribution to the stronger binding affinity is due to the stronger electrostatic interaction between NAD^+ and enzyme in term of ΔEEL in the component analysis in Table 2. The proximity of charged groups near negatively charged pyrophosphate moiety or positively charged nicotinamide moiety favors Sir2Tm, as observed from the interaction diagram between NAD^+ and the receptor (including both enzyme and peptide substrate) constructed from the averaged structure of last 10ps, e.g. ARG34 in Sir2Tm and ASP156 in SIRT3. Other polar interactions such hydrogen bonds also favors Sir2Tm/NAD^+ interactions. In the Sir2Tm ternary structure, more hydrogen bond interactions were formed between NAD^+ and receptor, and less exposure to solvent. It can also be found in the structural presentation of the binding sites. Also notable are the solvation energy losses. SIRT3 has less loss in solvation energy upon NAD^+ binding in the ternary complex, which can be seen from the interaction diagrams that NAD^+ in SIRT3 ternary complex has more exposure to solvent. However, the favorable solvation energy also leads to less favorable contacts between NAD^+ and enzyme/peptide substrate, resulting in lower binding affinity.

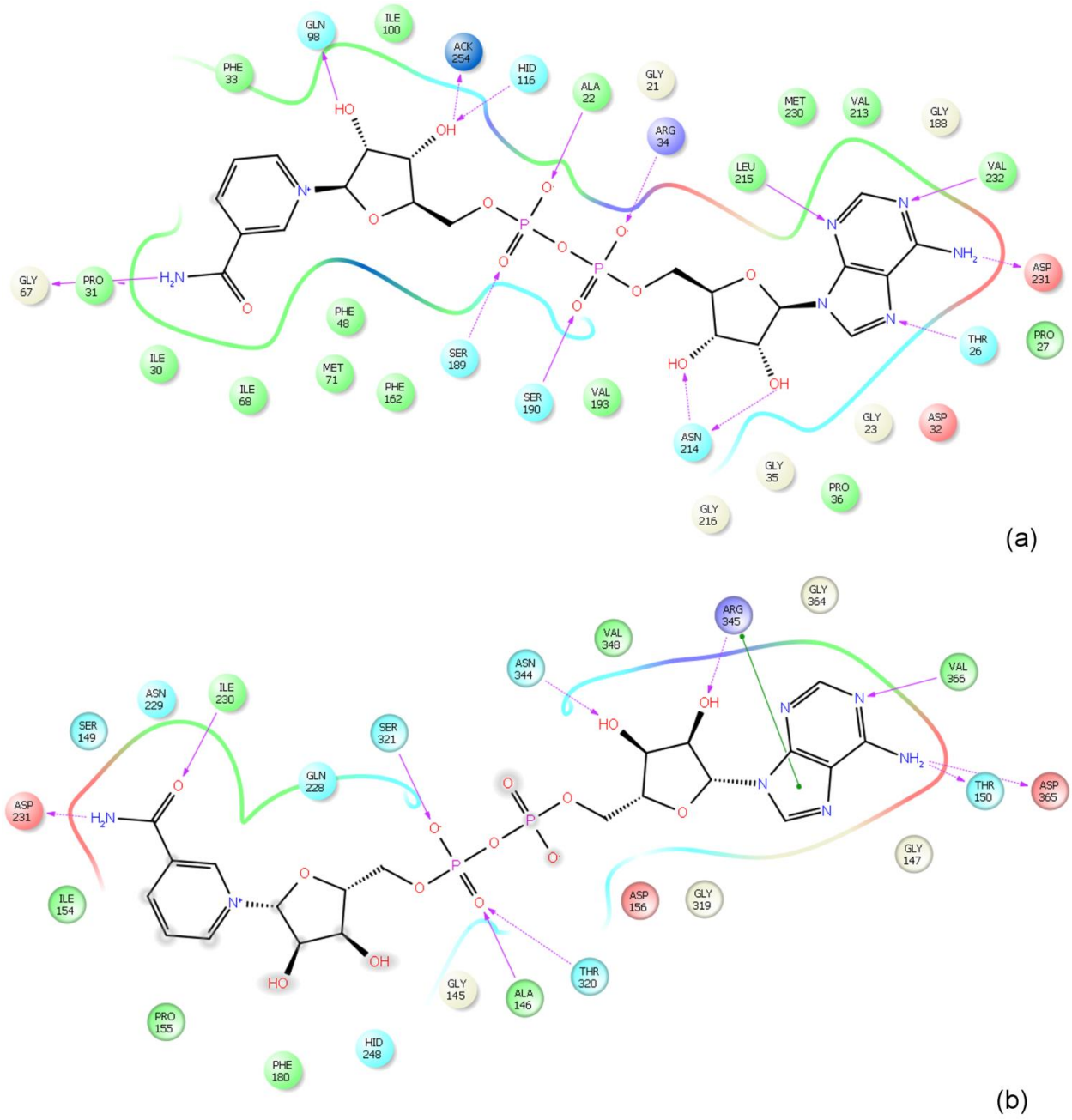

Figure 12. NAD$^+$ interaction diagrams. (a) Sir2Tm-NAD$^+$ interaction diagrams of MD averaged structures (10 frames from last 10ps) - ternary complex (Sir2Tm:Ac-p53:NAD$^+$); (b) SIRT3-NAD$^+$ interaction diagrams of MD averaged structures (10 frames from last 10ps) - ternary complex (SIRT3:Ac-CS2:NAD$^+$).

Due to the complex reaction mechanism of sirtuins, $K_{m,NAD+}$ does not provide an accurate estimate of $K_{d,NAD+}$. However, according to equation (5), the x-coordinate of the intersection

point of the double reciprocal plots at various [NAM] provides an estimate of $-\frac{1}{K_{d,NAD+}}\frac{1+K_{ex}}{K_{ex}}$, under the approximation $k_{cat} << k_j,\ \ j \neq cat$. Our binding affinity computations on SIRT3 are consistent with the position of the intersection point in Figure 2. With respect to the value of α, whereas in some enzymatic reactions, a larger dissociation constant of the substrate for a fixed value of k_{cat} leads to a higher ratio K_d/K_m, this does not necessarily always hold for sirtuins. The values of other rate constants, including the exchange rate constants, can play an important role in determining the extent of competition in NAM inhibition. Further studies exploring the extent to which weak NAD^+ binding correlates with competition in NAM inhibition kinetics are warranted and underway.

Prospects for Activation of SIRT3 by Derepression of NAM Inhibition

Sirtuins have evolved different strategies for both NAD^+ activation and NAM inhibition that suit their physiological roles [28,64]. Like Sir2, SIRT3 is potently inhibited by NAM. But the mechanistic details of this inhibition play a critical role in determining the scope of possible strategies that can activate SIRT3 by derepression of NAM inhibition.

Activation of sirtuins has been the subject of intense interest [26,50,65-67]. Understanding of the scope for activation of mammalian sirtuins is limited and structure-based design is challenging for allosteric activators [65]. Structure-based design of activators that operate via NAM derepression requires a detailed model of the inhibition mechanism.

Sauve et al. [27] provided an estimate for the base exchange equilibrium constant in mSIRT1 of about 20. Based on this estimate alone, the maximal possible activation of mSIRT1 by complete inhibition of the base exchange reaction at a given NAM concentration is higher than that of yeast Sir2, which has been successfully activated by competitive inhibitors of the base

exchange reaction, like isoNAM[26]. IsoNAM is a ligand that can compete with NAM for binding but cannot initiate the reverse reaction, thereby leading to apparent activation through relief of nicotinamide inhibition [26,68]. The data in Fig.5 show that addition of 900 μM isoNAM may slightly decrease the SIRT3 inhibition in the presence of 100 μM NAM. Computational, structural and further biochemical studies on these compounds and mechanisms might enable the development of sirtuin isoform selective modulators. In these strategies, competitive inhibition of the base exchange reaction must be possible without substantial competitive inhibition of the deacetylation reaction.

The information provided by NAM inhibition kinetics (e.g., the value of α) regarding the relative magnitudes of binding rate constants and other (e.g., reverse) rate constants in the reaction mechanism has implications for sirtuin activation by NAM derepression. In particular, an inert C pocket binding ligand I_2 will further increase the apparent $K_{m,NAD+}$ of the enzyme, so the value of α for NAM inhibition, which quantifies the effective competition between NAM and NAD^+ in the absence of activator, will affect the scope for activation through base exchange derepression. Note that the extent of overall competition does not depend solely on $K_{d,NAD+}$ and $K_{d,I2}$. Development of initial rate models for such reaction networks based on methods similar to those presented in this work could serve as a foundation for the rational computational design of sirtuin activators. By coupling to an appropriate computational model for binding affinity prediction based on MM-PB(GB)SA, computationally driven activator design may be possible. Similar methods could be applied to computationally screen for mutations that modulate base exchange inhibition through modification of $K_{d,NAM}$, for the purpose of understanding the selection pressures the drove the evolution of the diverse sensitivities of sirtuin enzyme active sites to NAM[69,70].

Hence the inhibition mode affects the scope for and establishes design criteria for sirtuin activation by NAM derepression. Mammalian sirtuins have evolved higher $K_{m,NAD+}$'s to function as NAD^+ sensors; SIRT1/SIRT3 may also have high K_{ex}'s, which result in the possibility of nearly complete inhibition by NAM at NAM concentrations significantly below NAM's K_d – hence allowing them to serve as good NAM sensors at low physiological concentrations of NAM. The evolution of these properties has been accompanied by different degrees of competitive behavior toward NAD^+ in the inhibition kinetics of NAM. Recent evidence suggests that certain symptoms of aging can be reversed in some mammals by sirtuin activation[16]; most of such work has considered increasing NAD^+ levels; reducing NAM inhibition may also be a viable strategy for activating certain mammalian sirtuins. The mechanistic understanding provided herein may be useful for clarifying the feasibility of a particular activation strategy.

For inhibition of the forward reaction, high values of α (e.g. for isoNAM) can be explained through simple competitive binding. However, SIRT3 data indicates that base exchange product inhibition can also display high values of α, which may originate in differences between $K_{m,NAD+}$ and $K_{d,NAD+}$ if the $k_{cat} << k_j, j \neq cat$ approximation is accurate. The difference between the $K_{m,NAD+}$ and $K_{d,NAD+}$ of a sirtuin may therefore be an important characteristic of its catalytic and inhibitory mechanisms that should be explored further. Steady state models are essential tools for understanding these differences and will be developed further in future work. Similar analyses could be carried out for other sirtuins, including mouse SIRT3. Future work should also involve QM/MM simulations and base exchange experiments[26] to more accurately estimate k_{ex}, k_{-ex} of mammalian sirtuins. More accurate binding affinity estimates of C pocket binding ligands can also be made using linear interaction methods on congeneric series [63].

Materials and Methods

Chemicals and Reagents

The acetylated substrate peptide based on the sequence of Acetyl-coenzyme A synthetase 2 (AceCS2 638-649, H2N-TRSGK (Ac)VMRRLLR-OH) was synthesized at PEPTIDE 2.0 Inc(Chantilly, VA, USA). Human recombinant SIRT3 was purchased from Creative BioMart(Shirley, NY, USA). Enzyme concentrations were determined using the method of Bradford[71] with bovine serum albumin (BSA) as the standard. All other chemicals used were of the highest purity commercially available and were purchased from Sigma (St. Louis, MO, USA), and Fisher Scientific (Pittsburgh, PA, USA).

Measurement of Deacetylation Activity Using a Fluorolabeled Peptide

The steady state parameters (K_m and k_{cat}) and catalytic efficiency (k_{cat}/K_m) of deacetylase activity of recombinant human SIRT1 and SIRT3 was determined using a fluorometric assay. The deacetylation activities were measured by using the SIRT3 Fluorimetic Drug Discovery Kit(AK 557, Enzo Life Sciences) and SIRT1 Fluorimetric Drug Discovery Kit (AK 555, Enzo Life Sciences). This assay system allows detection of a fluorescent signal upon deacetylation of an acetylated substrate peptide, comprising amino acids 317-320 of human p53 (Gln-Pro-Lys-Lys^{Ac}) for SIRT3 and 379-382 (Arg-His-Lys-Lys^{Ac}) for SIRT1 , when treated with developer. The intensity of fluorescence was measured on a fluorometric microplate reader (Fluoroskan Ascent® FL, Thermo LabSystems) with excitation set at 355 nm and emission detection set at 460 nm. The initial rate of the NAD^+-dependent deacetylation activity of SIRT3 enzyme was measured at different concentrations of nicotinamide adenine dinucleotide. The reactions were carried out at 37°C in a 50µl reaction volume containing 50 mM Tris/Cl (pH=8), 137 mM NaCl, and 100 µM

fluorolabeled peptide substrate. Unless otherwise indicated, all initial rate measurements were means of three or more replicates, obtained with single incubation times, at which point 5% or less of the substrate initially present had been deacetylated. The raw data were fitted to the Michaelis-Menten equation and defined inhibition models (Eqs. 1 and 2) by using GraphPad Prism (GraphPad Software, Inc, CA) to obtain the kinetic constants.

Measurement of IC_{50}Values for SIRT3 Inhibitor, NAM and isoNAM

This assay was also used to measure the inhibition by NAM, isoNAM and a combination of both. Reactions were performed in the presence of 100 μM NAD^+, and either NAM (0, 12.5, 25, 50, 100, 200, 500 μM) or 50 μM of NAM with isoNAM (0, 0.05, 0.1, 1, 5, and 10 mM). The initial rates were measured at different concentrations of NAM and isoNAM, and the reaction conditions were the same as above. The data were fitted to Equation 7 by using Prism to calculate the IC_{50} values:

$$v_i = v_0\left(1 - \frac{1}{IC_{50}+[I]}\right) \qquad (7)$$

Where v_0 is the initial rate of the uninhibited reaction and $v_i$is the initial rate of the reaction at concentration I of the inhibitor.

Measurement of the Relative Inhibition Effect of IsoNAM in the presence of NAM

The deacetylation activity was measured by using the SIRT3 Fluorimetric Drug Discovery Kit (AK 557, Enzo Life Sciences). In the presence of 100 uM of NAM, deacetylation activity of SIRT3 enzyme was measured under addition of different concentrations of isoNAM, range from 50 μM to 100 mM. The reactions were carried out at 37^{o}C in a 50 μl reaction volume containing 50 mM Tris/Cl (pH=8), 137 mM NaCl, and 100 μM fluorolabeled peptide substrate.

Molecular Dynamics Simulations of Ligand Binding

The crystal structure of SIRT3/Ac-CS2/Carba-NAD^+ (PBDID: 4FVT) was used as the starting structure to construct all the structures in SIRT3 MD simulations. Ternary complex was constructed by simply modifying Carba-NAD^+ to NAD^+ and replace norleucine with methionine as in the original sequence of Ac-CS2. SIRT3/NAD^+ binary structure was obtained by removing the peptide substrate from the ternary complex. For complex also including nicotinamide as inhibitor, NAD^+ and NAM coordinates were taken directly from crystal structure of Sir2Af2/NAD^+ complex (PBDID: 1YC2 chain A) after structural alignment between 4FVT and 1YC2:A. Complex including iso-nicotinamide = was built by modifying NAM to isoNAM in the above structure. All other molecules including waters were removed. Extra sodium and chloride ions were added to neutralize the system and maintain an ionic strength of about 0.06 M, followed by solvation using boxes of TIP3P water molecules with a margin of 12.0 Å from solute atoms in all three dimensions.

Models for SIRT3, Ac-CS2 and NAD^+ alone were also constructed by taking the coordinates of from 4FVT crystal structure, followed by the same neutralization and solvation process.

The crystal structure of Sir2Tm:Ac-p53:NAD^+ (PBDID: 2H4F) was used as that starting structure to construct all the structures in SIRT3 MD simulations. The missing loop of residue 37-42 was modeled using an ab initio loop prediction method in Prime version 3.2 (Schrödinger, LLC) during the protein preparation stage. Sir2Tm:NAD^+ binary structure was obtained by removing the peptide substrate from the ternary complex. Complex of Sir2Tm:Ac-p53:NAD^+:NAM was obtained by first removing the NAD^+, followed by superimposing the NAD^+ and NAM from 1YC2:A after structural alignment. All other molecules including waters

were removed, and extra sodium and chloride ions were added to maintain system neutrality. The complexes were then solvated using boxes of TIP3P water molecules with a margin of 12.0 Å from solute atoms.

The Amber99SB force field[72,73] was used for all the molecular mechanics calculations. Extra parameters were adapted from the following sources: parameters for Zn developed by Luo's group[74]; parameters for NAD^+ developed by Walker et al[75] and Pavelites et al[76]; parameters for acetylated lysine developed by Papamokos et al[77]. Charges for nicotinamide and isonicotinamide were derived from RESP fits to electrostatic potentials obtained at HF/6-31(d) level of theory that is consistent with Amber99SB force field.

All MD simulations were performed with the periodic boundary condition to produce isothermal-isobaric ensembles (NPT) at 300 K using the NAMD program[78]. The Particle Mesh Ewald (PME) method[79] was used to calculate the electrostatic energy. The covalent bonds involving hydrogen atoms were frozen with the SHAKE algorithm[80]. Temperature was regulated using the Langevin dynamics with the collision frequency of 1 ps^{-1}. Pressure regulation was achieved with isotropic position scaling and the pressure relaxation time was set to 1.0 picosecond. The integration of the equations of motion was conducted at a time step of 2 femtoseconds.

There are three phases in MD simulations. First in the relaxation phase, the system underwent a 2000-step minimization before a short 200 ps NPT MD simulation, with the main chain atoms of protein restrained to the positions of crystal structures with force constants of 5 kcal mol^{-1} $Å^{-2}$. Next, the systems ran for various lengths of time up to 22ns in the equilibration phase. Last, the sampling phase includes a 10ns of MD simulation.

Binding Affinity Estimation

Binding free energies were calculated using the MM-PBSA and the MM-GBSA methods as implemented in the AMBER package[81]. In MM-PBSA and MM-GBSA, binding free energy is evaluated as:

$$\Delta G_{\text{bind}} = \Delta E_{\text{MM}} + \Delta G_{\text{solv}} - T\Delta S \qquad (8)$$

where ΔE_{MM}, ΔG_{solv} and $T\Delta S$ are the changes of gas-phase interaction energy, solvation free energy, and solute conformational entropy change upon binding. ΔE_{MM} includes internal energy in bonded terms, electrostatic and van der Waals energies. ΔG_{solv} is the sum of polar contributions calculated using PB or GB model, and nonpolar contributions estimated from solvent-accessible surface area (SASA).

All the calculations were carried out using the MMPBSA.py module with AmberTools13[81]. The polar contribution of the solvation free energy was calculated by GB model developed by Onufriev et al.[82] and by PB method implemented in pbsa program. A salt concentration of 0.1M was used in MM-GBSA calculations. The solvent-accessible surface area was evaluated using the LCPO method[83]. Because relative free energy trends were of interest, solute conformational entropy change was neglected. Energies were evaluated using 10000 snapshots extracted from the last 10 ns at time interval of 1 ps of each trajectory after ensuring that each one of these trajectories was completely stable. One exception is the highly dynamic SIRT3/NAD^+ binary system, where 20000 snapshots from last 20 ns were used in energy evaluations.

References

1. Minino AM, Murphy SL, Xu J, Kochanek KD (2011) Deaths: final data for 2008. National vital statistics reports : from the Centers for Disease Control and Prevention, National Center for Health Statistics, National Vital Statistics System 59: 1-126.
2. Kaeberlein M, McVey M, Guarente L (1999) The SIR2/3/4 complex and SIR2 alone promote longevity in Saccharomyces cerevisiae by two different mechanisms. Genes & Development 13: 2570-2580.
3. Lin SJ, Defossez PA, Guarente L (2000) Requirement of NAD and SIR2 for life-span extension by calorie restriction in Saccharomyces cerevisiae. Science 289: 2126-2128.
4. Frye RA (1999) Characterization of five human cDNAs with homology to the yeast SIR2 gene: Sir2-like proteins (sirtuins) metabolize NAD and may have protein ADP-ribosyltransferase activity. Biochemical and Biophysical Research Communications 260: 273-279.
5. Frye RA (2000) Phylogenetic classification of prokaryotic and eukaryotic Sir2-like proteins. Biochemical and Biophysical Research Communications 273: 793-798.
6. Onyango P, Celic I, McCaffery JM, Boeke JD, Feinberg AP (2002) SIRT3, a human SIR2 homologue, is an NAD-dependent deacetylase localized to mitochondria. Proceedings of the National Academy of Sciences of the United States of America 99: 13653-13658.
7. Lombard DB, Alt FW, Cheng HL, Bunkenborg J, Streeper RS, et al. (2007) Mammalian sir2 homolog SIRT3 regulates global mitochondrial lysine acetylation. Molecular and Cellular Biology 27: 8807-8814.
8. Hallows WC, Lee S, Denu JM (2006) Sirtuins deacetylate and activate mammalian acetyl-CoA synthetases. Proceedings of the National Academy of Sciences of the United States of America 103: 10230-10235.
9. Schwer B, Bunkenborg J, Verdin RO, Andersen JS, Verdin E (2006) Reversible lysine acetylation controls the activity of the mitochondrial enzyme acetyl-CoA synthetase 2. Proceedings of the National Academy of Sciences of the United States of America 103: 10224-10229.
10. Hallows WC, Yu W, Smith BC, Devires MK, Ellinger JJ, et al. (2011) Sirt3 Promotes the Urea Cycle and Fatty Acid Oxidation during Dietary Restriction. Molecular Cell 41: 139-149.
11. Hirschey MD, Shimazu T, Goetzman E, Jing E, Schwer B, et al. (2010) SIRT3 regulates mitochondrial fatty-acid oxidation by reversible enzyme deacetylation. Nature 464: 121-U137.
12. Lu ZP, Bourdi M, Li JH, Aponte AM, Chen Y, et al. (2011) SIRT3-dependent deacetylation exacerbates acetaminophen hepatotoxicity. Embo Reports 12: 840-846.
13. Guarente L (2014) Sirtuins and the Warburg effect. Nature Medicine 20: 24-25.
14. Finley LWS, Carracedo A, Lee J, Souza A, Egia A, et al. (2011) SIRT3 Opposes Reprogramming of Cancer Cell Metabolism through HIF1 alpha Destabilization. Cancer Cell 19: 416-428.
15. Sauve AA (2010) Sirtuin chemical mechanisms. Biochimica Et Biophysica Acta-Proteins and Proteomics 1804: 1591-1603.
16. Gomes AP, Price NL, Ling AJY, Moslehi JJ, Montgomery MK, et al. (2013) Declining NAD(+) Induces a Pseudohypoxic State Disrupting Nuclear-Mitochondrial Communication during Aging. Cell 155: 1624-1638.
17. Massudi H, Grant R, Braidy N, Guest J, Farnsworth B, et al. (2012) Age-Associated Changes In Oxidative Stress and NAD(+) Metabolism In Human Tissue. Plos One 7.
18. Canto C, Houtkooper RH, Pirinen E, Youn DY, Oosterveer MH, et al. (2012) The NAD(+) Precursor Nicotinamide Riboside Enhances Oxidative Metabolism and Protects against High-Fat Diet-Induced Obesity. Cell Metabolism 15: 838-847.

19. Mouchiroud L, Houtkooper RH, Moullan N, Katsyuba E, Ryu D, et al. (2013) The NAD(+)/Sirtuin Pathway Modulates Longevity through Activation of Mitochondrial UPR and FOXO Signaling. Cell 154: 430-441.
20. Ramsey KM, Yoshino J, Brace CS, Abrassart D, Kobayashi Y, et al. (2009) Circadian Clock Feedback Cycle Through NAMPT-Mediated NAD(+) Biosynthesis. Science 324: 651-654.
21. Berger F, Ramirez-Hernandez MH, Ziegler M (2004) The new life of a centenarian: signalling functions of NAD(P). Trends in Biochemical Sciences 29: 111-118.
22. Dietrich LS (1971) REGULATION OF NICOTINAMIDE METABOLISM. American Journal of Clinical Nutrition 24: 800-&.
23. Smythe GA, Braga O, Brew BJ, Grant RS, Guillemin GJ, et al. (2002) Concurrent quantification of quinolinic, picolinic, and nicotinic acids using electron-capture negative-ion gas chromatography-mass spectrometry. Analytical Biochemistry 301: 21-26.
24. Hagino Y, Lan SJ, Ng CY, Henderso.Lm (1968) METABOLISM OF PYRIDINIUM PRECURSORS OF PYRIDINE NUCLEOTIDES IN PERFUSED RAT LIVER. Journal of Biological Chemistry 243: 4980-&.
25. Avalos JL, Boeke JD, Wolberger C (2004) Structural basis for the mechanism and regulation of Sir2 enzymes. Molecular Cell 13: 639-648.
26. Sauve AA, Moir RD, Schramm VL, Willis IM (2005) Chemical activation of Sir2-dependent silencing by relief of nicotinamide inhibition. Molecular Cell 17: 595-601.
27. Sauve AA, Schramm VL (2003) Sir2 regulation by nicotinamide results from switching between base exchange and deacetylation chemistry. Biochemistry 42: 9249-9256.
28. Fischer F, Gertz M, Suenkel B, Lakshminarasimhan M, Schutkowski M, et al. (2012) Sirt5 Deacylation Activities Show Differential Sensitivities to Nicotinamide Inhibition. Plos One 7.
29. Jin L, Galonek H, Israelian K, Choy W, Morrison M, et al. (2009) Biochemical characterization, localization, and tissue distribution of the longer form of mouse SIRT3. Protein Science 18: 514-525.
30. Hou T, Wang J, Li Y, Wang W (2011) Assessing the performance of the molecular mechanics/Poisson Boltzmann surface area and molecular mechanics/generalized Born surface area methods. II. The accuracy of ranking poses generated from docking. J Comput Chem 32: 866-877.
31. Rastelli G, Rio AD, Degliesposti G, Sgobba M (2010) Fast and accurate predictions of binding free energies using MM-PBSA and MM-GBSA. Journal of Computational Chemistry 31: 797-810.
32. Guimarães CRW, Cardozo M (2008) MM-GB/SA Rescoring of Docking Poses in Structure-Based Lead Optimization. J Chem Inf Model.
33. Lyne PD, Lamb ML, Saeh JC (2006) Accurate Prediction of the Relative Potencies of Members of a Series of Kinase Inhibitors Using Molecular Docking and MM-GBSA Scoring. J Med Chem 49: 4805-4808.
34. Copeland RA (2005) Evaluation of enzyme inhibitors in drug discovery: a guide for medicinal chemists and pharmacologists. New Jersey: A John Wiley & Sons, Inc. 271 p.
35. Rye PT, Frick LE, Ozbal CC, Lamarr WA (2011) Advances in Label-Free Screening Approaches for Studying Sirtuin-Mediated Deacetylation. Journal of Biomolecular Screening 16: 1217-1226.
36. Grubisha O, Smith BC, Denu JM (2005) Small molecule regulation of Sir2 protein deacetylases. Febs Journal 272: 4607-4616.
37. Jackson MD, Schmidt MT, Oppenheimer NJ, Denu JM (2003) Mechanism of nicotinamide inhibition and transglycosidation by Sir2 histone/protein deacetylases. Journal of Biological Chemistry 278: 50985-50998.
38. Cosgrove MS, Bever K, Avalos JL, Muhammad S, Zhang XB, et al. (2006) The structural basis of sirtuin substrate affinity. Biochemistry 45: 7511-7521.
39. Jin L, Wei WT, Jiang YB, Peng H, Cai JH, et al. (2009) Crystal Structures of Human SIRT3 Displaying Substrate-induced Conformational Changes. Journal of Biological Chemistry 284: 24394-24405.
40. Zhao X, Allison D, Condon B, Zhang FY, Gheyi T, et al. (2013) The 2.5 angstrom Crystal Structure of the SIRT1 Catalytic Domain Bound to Nicotinamide Adenine Dinucleotide (NAD(+)) and an Indole (EX527 Analogue) Reveals a Novel Mechanism of Histone Deacetylase Inhibition. Journal of Medicinal Chemistry 56: 963-969.
41. Davenport AM, Huber FM, Hoelz A (2014) Structural and functional analysis of human SIRT1. J Mol Biol 426: 526-541.
42. Avalos JL, Bever KM, Wolberger C (2005) Mechanism of sirtuin inhibition by nicotinamide: Altering the NAD(+) cosubstrate specificity of a Sir2 enzyme. Molecular Cell 17: 855-868.
43. North BJV, E. (2004) Sirtuins: Sir2-related NAD-dependent protein deacetylases. Genome Biology 5: 224.

44. Bitterman KJ, Anderson RM, Cohen HY, Latorre-Esteves M, Sinclair DA (2002) Inhibition of silencing and accelerated aging by nicotinamide, a putative negative regulator of yeast Sir2 and human SIRT1. Journal of Biological Chemistry 277: 45099-45107.
45. Giralt A, Villarroya F (2012) SIRT3, a pivotal actor in mitochondrial functions: metabolism, cell death and aging. Biochemical Journal 444: 1-10.
46. Cen Y (2010) Sirtuins inhibitors: The approach to affinity and selectivity. Biochimica Et Biophysica Acta-Proteins and Proteomics 1804: 1635-1644.
47. Imai S, Yoshino J (2013) The importance of NAMPT/NAD/SIRT1 in the systemic regulation of metabolism and ageing. Diabetes Obesity & Metabolism 15: 26-33.
48. Yang HY, Yang T, Baur JA, Perez E, Matsui T, et al. (2007) Nutrient-sensitive mitochondrial NAD(+) levels dictate cell survival. Cell 130: 1095-1107.
49. Peek CB, Nati AHA, Ramsey KM, Kuo HY, Yu W, et al. (2013) Circadian Clock NAD(+) Cycle Drives Mitochondrial Oxidative Metabolism in Mice. Science 342: 591-+.
50. Feldman JL, Baeza J, Denu JM (2013) Activation of the Protein Deacetylase SIRT6 by Long-chain Fatty Acids and Widespread Deacylation by Mammalian Sirtuins. Journal of Biological Chemistry 288: 31350-31356.
51. Schmidt MT, Smith BC, Jackson MD, Denu JM (2004) Coenzyme specificity of Sir2 protein deacetylases - Implications for physiological regulation. Journal of Biological Chemistry 279: 40122-40129.
52. Tervo AJ, Kyrylenko S, Niskanen P, Salminen A, Leppanen J, et al. (2004) An in silico approach to discovering novel inhibitors of human sirtuin type 2. Journal of Medicinal Chemistry 47: 6292-6298.
53. Anderson RM, Bitterman KJ, Wood JG, Medvedik O, Sinclair DA (2003) Nicotinamide and PNC1 govern lifespan extension by calorie restriction in Saccharomyces cerevisiae. Nature 423: 181-185.
54. Adams JD, Klaidman LK (2007) Sirtuins, nicotinamide and aging: A critical review. Letters in Drug Design & Discovery 4: 44-48.
55. Qin WP, Yang TL, Ho L, Zhao Z, Wang J, et al. (2006) Neuronal SIRT1 activation as a novel mechanism underlying the prevention of Alzheimer disease amyloid neuropathology by calorie restriction. Journal of Biological Chemistry 281: 21745-21754.
56. Segel IH (1993) Enzyme Kinetics Behavior and analysis of rapid equilibrium and steady-state enzyme systems. USA: Wiley Classics Library. 957 p.
57. Shi YW, Zhou YZ, Wang SL, Zhang YK (2013) Sirtuin Deacetylation Mechanism and Catalytic Role of the Dynamic Cofactor Binding Loop. Journal of Physical Chemistry Letters 4: 491-495.
58. Sauve AA, Schramm VL (2003) Nicotinamide inhibition of SIR2 is a consequence of chemical competition for an ADPR - peptidyl intermediate. Biochemistry 42: 8630-8630.
59. Hu P, Wang SL, Zhang YK (2008) Highly Dissociative and Concerted Mechanism for the Nicotinamide Cleavage Reaction in Sir2Tm Enzyme Suggested by Ab Initio QM/MM Molecular Dynamics Simulations. Journal of the American Chemical Society 130: 16721-16728.
60. Liang ZJ, Shi T, Ouyang SS, Li HL, Yu KQ, et al. (2010) Investigation of the Catalytic Mechanism of Sir2 Enzyme with QM/MM Approach: SN1 vs SN2? Journal of Physical Chemistry B 114: 11927-11933.
61. Cer RZ, Mudunuri U, Stephens R, Lebeda FJ (2009) IC50-to-K-i: a web-based tool for converting IC50 to K-i values for inhibitors of enzyme activity and ligand binding. Nucleic Acids Research 37: W441-W445.
62. Rastelli G, Del Rio A, Degliesposti G, Sgobba M (2010) Fast and Accurate Predictions of Binding Free Energies Using MM-PBSA and MM-GBSA. Journal of Computational Chemistry 31: 797-810.
63. Aqvist J, Luzhkov VB, Brandsdal BO (2002) Ligand binding affinities from MD simulations. Accounts of Chemical Research 35: 358-365.
64. Verdin E (2014) Coupling of NAD metabolism, sirtuins and lifespan. Nature Medicine 20: 25-27.
65. Hubbard BP, Gomes AP, Dai H, Li J, Case AW, et al. (2013) Evidence for a Common Mechanism of SIRT1 Regulation by Allosteric Activators. Science 339: 1216-1219.
66. Milne JC, Lambert PD, Schenk S, Carney DP, Smith JJ, et al. (2007) Small molecule activators of SIRT1 as therapeutics for the treatment of type 2 diabetes. Nature 450: 712-716.
67. Howitz KT, Bitterman KJ, Cohen HY, Lamming DW, Lavu S, et al. (2003) Small molecule activators of sirtuins extend Saccharomyces cerevisiae lifespan. Nature 425: 191-196.
68. Cen Y, Youn DY, Sauve AA (2011) Advances in Characterization of Human Sirtuin Isoforms: Chemistries, Targets and Therapeutic Applications. Current Medicinal Chemistry 18: 1919-1935.
69. Chakrabarti R, Klibanov AM, Friesner RA (2005) Sequence optimization and designability of enzyme active sites. Proceedings of the National Academy of Sciences of the United States of America 102: 12035-12040.

70. Chakrabarti R, Klibanov AM, Friesner RA (2005) Computational prediction of native protein-ligand binding and enzyme active site sequences. Proceedings of the National Academy of Sciences of the United States of America 102: 10153-10158.
71. Bradford MM (1976) RAPID AND SENSITIVE METHOD FOR QUANTITATION OF MICROGRAM QUANTITIES OF PROTEIN UTILIZING PRINCIPLE OF PROTEIN-DYE BINDING. Analytical Biochemistry 72: 248-254.
72. Hornak V, Abel R, Okur A, Strockbine B, Roitberg A, et al. (2006) Comparison of multiple amber force fields and development of improved protein backbone parameters. Proteins-Structure Function and Bioinformatics 65: 712-725.
73. Wang JM, Cieplak P, Kollman PA (2000) How well does a restrained electrostatic potential (RESP) model perform in calculating conformational energies of organic and biological molecules? Journal of Computational Chemistry 21: 1049-1074.
74. Lu Q, Tan YH, Luo R (2007) Molecular dynamics simulations of p53 DNA-binding domain. Journal of Physical Chemistry B 111: 11538-11545.
75. Walker RC, de Souza MM, Mercer IP, Gould IR, Klug DR (2002) Large and fast relaxations inside a protein: Calculation and measurement of reorganization energies in alcohol dehydrogenase. Journal of Physical Chemistry B 106: 11658-11665.
76. Pavelites JJ, Gao JL, Bash PA, Mackerell AD (1997) A molecular mechanics force field for NAD(+), NADH, and the pyrophosphate groups of nucleotides. Journal of Computational Chemistry 18: 221-239.
77. Papamokos GV, Tziatzos G, Papageorgiou DG, Georgatos SD, Politou AS, et al. (2012) Structural Role of RKS Motifs in Chromatin Interactions: A Molecular Dynamics Study of HP1 Bound to a Variably Modified Histone Tail. Biophysical Journal 102: 1926-1933.
78. Phillips JC, Braun R, Wang W, Gumbart J, Tajkhorshid E, et al. (2005) Scalable molecular dynamics with NAMD. Journal of Computational Chemistry 26: 1781-1802.
79. Darden T, York D, Pedersen L (1993) PARTICLE MESH EWALD - AN N.LOG(N) METHOD FOR EWALD SUMS IN LARGE SYSTEMS. Journal of Chemical Physics 98: 10089-10092.
80. Ryckaert JP, Ciccotti G, Berendsen HJC (1977) NUMERICAL-INTEGRATION OF CARTESIAN EQUATIONS OF MOTION OF A SYSTEM WITH CONSTRAINTS - MOLECULAR-DYNAMICS OF N-ALKANES. Journal of Computational Physics 23: 327-341.
81. Miller BR, McGee TD, Swails JM, Homeyer N, Gohlke H, et al. (2012) MMPBSA.py: An Efficient Program for End-State Free Energy Calculations. Journal of Chemical Theory and Computation 8: 3314-3321.
82. Onufriev A, Bashford D, Case DA (2004) Exploring protein native states and large-scale conformational changes with a modified generalized born model. Proteins-Structure Function and Bioinformatics 55: 383-394.
83. Weiser J, Shenkin PS, Still WC (1999) Approximate atomic surfaces from linear combinations of pairwise overlaps (LCPO). Journal of Computational Chemistry 20: 217-230.

Figure Legends

Figure 1. Inhibition of SIRT3/SIRT1 by nicotinamide and its analog. (A) Nicotinamide / isonicotinamide inhibition assays showing percent change in deacetylation activity as a function of NAM/isoNAM concentration. Data for the SIRT1 enzyme are indicated with closed squares and a blue curve; data for the SIRT3 enzyme are indicated with filled circles and a red line. **(B)** The inset table lists the IC_{50}s of the two inhibitors for these enzymes.

Figure 2. Inhibition of SIRT3/SIRT1 against NAD^+ by Nicotinamide. (**A**) Recombinant human SIRT1 was incubated for 0, 10, 20, 30, 60, 120, 180, and 240 min at 37^{o}C in the presence of 50, 125, 750, 1500 μM NAD^+ and 0, 50, and 100 μM NAM. **(B)** Recombinant human SIRT3 was incubated for 0, 10, 20, 30, 60, 120, 180, and 240 min at 37^{o}C in the presence of 100, 375, 750, 1500, 3000 μM NAD^+ and 0, 25, 100, and 200 μM NAM. Reactions were terminated by the addition of developer and samples were analyzed by fluorometry (excitation set at 355 nm and emission at 460 nm). Data are globally nonlinear fitted to base exchange inhibition model (Eq. 1) and shown as a double-reciprocal plot of arbitrary fluorescence units (AFU) min^{-1} versus $1/[NAD^+]$ μM^{-1}.

Figure 3. Deacetylation rate as a function of nicotinamide concentration. Dixon plot ($1/v$ vs [*NAM*]) of the deacetylation rates for **(A)** SIRT1 and **(B)** SIRT3 enzymes. Experimental data were fit to a linear equation.

Figure 4. Inhibition of SIRT3 against NAD^+ by Isonicotinamide. Recombinant human SIRT3 was incubated for 0, 10, 20, 30, 60, 120, 180, and 240 min at 37°C in the presence of 100, 375, 750, 1500, 3000 μM NAD^+ and 0, 2.5, 10, and 40 mM isoNAM. Reactions were terminated by the addition of developer and samples were analyzed by fluorometry (excitation set at 355 nm and emission at 460 nm). Data are globally nonlinear fitted to mixed inhibition model (Eq. 2) and shown as a double-reciprocal plot of arbitrary fluorescence units (AFU) min^{-1} versus $1/[NAD^+]$ μM^{-1}.

Figure 5. Inhibition of SIRT3/SIRT1 by nicotinamide in the presence of IsoNAM. Recombinant human SIRT3 was incubated with 50, 500, 700 and 900 μM of isoNAM for 40 min at 37°C in the presence of 500 μM NAD^+, and 100 μM NAM. Reactions were terminated by the addition of developer and samples were analyzed by fluorometry (excitation set at 355 nm and emission at 460 nm).

Figure 6. Alignment of ternary complex (Sir2Tm:Ac-p53:NAD^+) from MD averaged structure with respect to crystal structure. Ribbon representation of crystal structure (PDB ID: 2H4F) is colored by secondary structure (sheets in cyan, helixes in red and coils in gray), MD averaged structure (10 frames over last 10ps) in yellow green color. Carbon atoms in crystal structure are in white, and are in yellow green for MD averaged structure. Alignment was made using residues 15-27, 182-242, which forms the stable A binding pocket in Rossmann fold domain.

Figure 7. A B, and C pockets of the MD averaged structure of Sir2Tm complex with NAM (Sir2Tm:Ac-p53:NAD^+:NAM). Carbon is colored in yellow for MD averaged structure of 10 frames over last 10 ps, in yellow green for reference NAD^+ structure from MD averaged structure over last 10 ps of Sir2Tm ternary complex.

Figure 8. A, B and C binding pockets identified in MD averaged structure of different SIRT3 complexes. (a) A and C pockets from the MD averaged structure of 10 frames over last 10 ps of ternary complex (SIRT3:Ac-CS2:NAD^+, carbon in yellow green), reference NAD^+ structure (carbon in white) from crystal structure 4FVT; (b) A, B and C pockets from the MD averaged structure of 10 frames over last 10 ps of SIRT3 complex with NAM (SIRT3:Ac-ACS2:NAD^+:NAM, carbon in yellow), reference NAD^+ structure (carbon in yellow green) from MD averaged structure over last 10 ps of SIRT3 ternary complex; (c) A, B and C pockets from the MD averaged structure of 10 frames over last 10 ps of SIRT3 complex with isoNAM (SIRT3:Ac-ACS2:NAD^+:isoNAM, carbon in plum), reference NAD^+ structure (carbon in yellow) from MD averaged structure over last 10 ps of SIRT3 complex with NAM.

Figure 9. General model for the inhibition of sirtuins by NAM. (A) Reaction scheme for the sirtuin deacetylation reaction and base exchange inhibition. For simplicity, deacetylation and AADPR + Pr dissociation are assumed to occur together (k_{cat} denotes the rate constant for deacetylation and dissociation of AADPR + Pr from E). **(B)** Simplified reaction network for base exchange inhibition. In the presence of saturating Ac-Pr, E is rapidly converted into E·Ac-Pr and NAM binding to E can be neglected, resulting in a simplified reaction network with 5 species. ADPR, adenosine diphosphate ribose; AADPR, O-acetyl-adenosine-diphosphate-ribose.

Figure 10. Mixed noncompetitive base exchange inhibition kinetics of sirtuin enzymes: mechanistic interpretation.

Figure 11. NAM/isoNAM interaction diagrams of MD averaged structures. (10 frames from last 10ps) (a) SIRT3 complex with NAM; (b) SIRT3 complex with isoNAM.

Figure 12. NAD^+ interaction diagrams. (a) Sir2Tm-NAD^+ interaction diagrams of MD averaged structures (10 frames from last 10ps) - ternary complex (Sir2Tm:Ac-p53:NAD^+); (b) SIRT3-NAD^+ interaction diagrams of MD averaged structures (10 frames from last 10ps) - ternary complex (SIRT3:Ac-CS2:NAD^+);

Supporting Information Legends

Figure S1. Snapshots taken from MD simulations of SIRT3:NAD^+ binary complex. Averaged structures of 10 frames over 10 ps at 22, 24, 26, 28, 30 and 32 ns from MD simulation of binary complex (SIRT3:NAD^+). Alignment was made using residues 139-151, 313-378 in Rossmann fold domain that forms A binding pocket with respect to SIRT3 ternary complex crystal structure 4FVT.

Figure S2. NAM interaction diagrams of MD averaged structures (10 frames from last 10ps) of Sir2TM complex with NAM.

Table 1. Model parameter estimates from global nonlinear fitting of mixed inhibition models for SIRT3 and SIRT1 inhibition by isoNAM (equation 2) and NAM (equation 1).

	Inhibitor	$K_{m,NAD+}$, μM	V_{max}, μM/min	$K_2(K_i)$	α
SIRT3	isoNAM	1402	27.83	(4623)	8.87E+18
	NAM	673.3	32.96	29.4	2.735
SIRT1	NAM	168.2	7.30	51.3	0.848

Table 2.MD/MM-PB(GB)SA binding affinity estimates for NAD^+ in SIRT3:Ac-CS2:$NAD^+$and Sir2Tm:Ac-p53:NAD^+ in catalytically productive (without NAM) binding mode.

	SIRT3:Ac-CS2:NAD^+		Sir2Tm:Ac-p53:NAD^+	
	Average	Std. Dev.	Average	Std. Dev.
ΔVDWAALS	-68.85	4.82	-78.24	4.71
ΔEEL	-2.14	18.13	-142.87	11.80
ΔEGB	14.13	15.11	125.91	8.05
ΔESURF	-8.76	0.25	-10.28	0.16
ΔEPB	24.47	15.75	152.11	8.21
ΔENPOLAR	-46.14	1.10	-51.62	0.66
ΔEDISPER	87.31	1.58	97.43	0.98
ΔG_gas	-70.99	17.71	-221.11	11.07
ΔG_solv_igb2	5.36	15.11	115.64	8.02
ΔG_solv_pb	65.64	16.00	197.92	8.26
ΔG_igb2	**-65.63**	**5.91**	**-105.48**	**6.48**
ΔG_pb	**-5.35**	**8.37**	**-23.19**	**7.27**

VDWAALS: van der waals not including the 1-4 terms
EEL: electrostatic interactions not including the 1-4 terms
EGB: Polar contribution to solvation energy by GB method
ESURF: non-polar contribution to solvation energy using SASA (solvent accessible surface area) for GB
EPB: Polar contribution to solvation energy by PB method
ENPOLAR: non-polar contribution to solvation energy from repulsive solute-solvent interactions for PB
EDISPER: non-polar contribution to solvation energy from attractive solute-solvent interactions for PB
G_gas: Gas phase MM energy including all bonded and non-bonded terms
G_solv_igb2: Total solvation energy by GB method
G_solv_pb: Total solvation energy by PB method

ΔG_igb2: Difference in total energy including gas phase MM energy and solvation energy by GB method
ΔG_pb: Difference in total energy including gas phase MM energy and solvation energy by PB method

Table 3. MD/MM-PB(GB)SA binding affinity estimates for NAD^+ in SIRT3:Ac-CS2:NAD^+ and Sir2Tm:Ac-p53:NAD^+ in catalytically unproductive (with NAM) binding modes.

	SIRT3:Ac-CS2:NAD^+:NAM		Sir2Tm:Ac-p53:NAD^+:NAM	
	Average	Std. Dev.	Average	Std. Dev.
ΔVDWAALS	-72.94	4.35	-72.40	4.57
ΔEEL	52.57	13.53	-82.21	20.85
ΔEGB	-33.94	12.02	81.85	15.75
ΔESURF	-8.81	0.28	-9.03	0.33
ΔEPB	-27.80	12.52	96.05	18.91
ΔENPOLAR	-44.93	1.14	-47.08	1.44
ΔEDISPER	85.00	1.46	89.48	1.83
ΔG_gas	-20.37	13.27	-154.60	21.64
ΔG_solv_igb2	-42.76	12.10	72.82	15.62
ΔG_solv_pb	12.27	12.58	138.45	19.06
ΔG_igb2	**-63.12**	**4.37**	**-81.78**	**8.01**
ΔG_pb	**-8.10**	**5.71**	**-16.15**	**8.35**

Table 4. MD/MM-PB(GB)SA binding affinity estimates for NAM and isoNAM in SIRT3:Ac-CS2:NAD^+ and Sir2Tm:Ac-p53:NAD^+

	SIRT3:Ac-CS2: NAD^+:NAM		Sir2Tm:Ac-p53: NAD^+:NAM		SIRT3:Ac-CS2: NAD^+:isoNAM	
	Average	Std. Dev.	Average	Std. Dev.	Average	Std. Dev.
ΔVDWAALS	-20.34	1.90	-19.94	1.87	-19.46	2.32
ΔEEL	-24.10	2.84	-18.48	2.95	-11.58	3.69
ΔEGB	27.51	1.64	20.57	1.69	18.10	2.02
ΔESURF	-2.89	0.08	-2.88	0.08	-2.75	0.16
ΔEPB	33.96	2.84	22.49	2.98	23.94	2.93
ΔENPOLAR	-14.47	0.25	-14.44	0.28	-13.49	0.59
ΔEDISPER	25.20	0.59	24.60	0.64	24.47	0.93
ΔG_gas	-44.44	2.59	-38.42	2.84	-31.04	3.67
ΔG_solv_igb2	24.62	1.63	17.69	1.67	15.35	2.01
ΔG_solv_pb	44.70	3.20	32.65	3.15	34.92	3.33
ΔG_igb2	**-19.82**	**1.89**	**-20.74**	**2.05**	**-15.68**	**2.48**
ΔG_pb	**0.26**	**3.26**	**-5.78**	**3.51**	**3.89**	**4.18**